The final publication is available at Elsevier via http://dx.doi.org/10.1016/j.nanoen.2018.05.049 © 2018. This manuscript version is made available under the CC-BY-NC-ND 4.0 license http://creativecommons.org/licenses/by-nc-nd/4.0/

Author's Accepted Manuscript

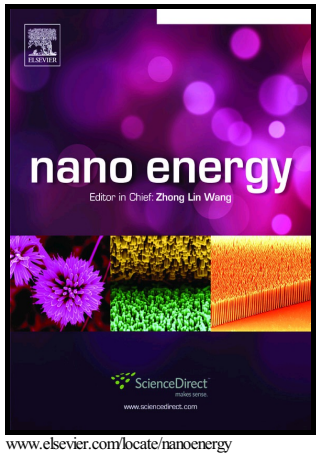

www.elsevier.com/locate/nanoenergy

Aqueous Intercalation-type Electrode Materials for Grid-level Energy Storage: Beyond the Limits of Lithium and Sodium

Zhenyu Xing, Shun Wang, Aiping Yu, Zhongwei Chen

PII: S2211-2855(18)30364-1
DOI: https://doi.org/10.1016/j.nanoen.2018.05.049
Reference: NANOEN2757

To appear in: *Nano Energy*

Received date: 27 April 2018
Revised date: 16 May 2018
Accepted date: 19 May 2018

Cite this article as: Zhenyu Xing, Shun Wang, Aiping Yu and Zhongwei Chen, Aqueous Intercalation-type Electrode Materials for Grid-level Energy Storage: Beyond the Limits of Lithium and Sodium, *Nano Energy,* https://doi.org/10.1016/j.nanoen.2018.05.049

This is a PDF file of an unedited manuscript that has been accepted for publication. As a service to our customers we are providing this early version of the manuscript. The manuscript will undergo copyediting, typesetting, and review of the resulting galley proof before it is published in its final citable form. Please note that during the production process errors may be discovered which could affect the content, and all legal disclaimers that apply to the journal pertain.

ACCEPTED MANUSCRIPT

Aqueous Intercalation-type Electrode Materials for Grid-level Energy Storage: Beyond the Limits of Lithium and Sodium

Zhenyu Xing,[a] Shun Wang[b]*, Aiping Yu,[a] and Zhongwei Chen[a]*

[a]Department of Chemical Engineering, Waterloo Institute for Nanotechnology, Waterloo Institute for Sustainable Energy, University of Waterloo, 200 University Avenue W, Waterloo, Ontario N2L 3G1, Canada

[b]Nanomaterials and Chemistry Key Laboratory, Wenzhou University, Wenzhou 325027, P. R. China

E-mail: zhwchen@uwaterloo.ca; shunwang@wzu.edu.cn

Accepted manuscript

Abstract

Intermittent, fluctuational, and unpredictable features of renewable energy require grid-level energy storage (GES). Among various types of GES, aqueous electrochemical storage is undoubtedly the most promising method due to its high round-trip efficiency, long cycle life, low cost and high safety. As the most encouraging candidate for aqueous electrochemical storage, aqueous rocking-chair batteries have been heavily investigated. Recently, intercalation-type aqueous batteries beyond the limits of Li^+ and Na^+ have caught researchers' attention due to potentially higher capacity and better cyclability, and the number of publications in this nascent field since 2015 has dramatically increased. Therefore, it is highly demanded to summarize what have been learned in this field. In this first comprehensive review paper, we summarize these novel intercalation-type electrode materials and provide perspectives of opportunities and challenges for future research.

ACCEPTED MANUSCRIPT

Graphical abstract

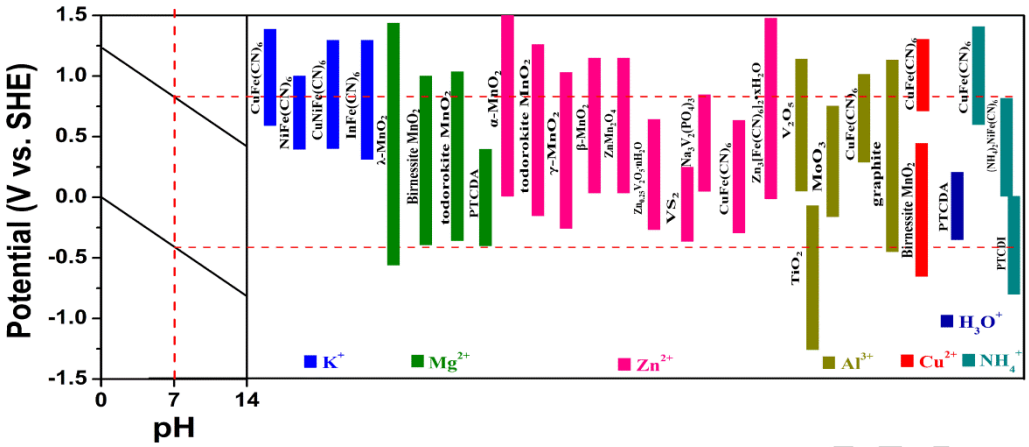

Key Words:

Grid-level energy storage, Aqueous batteries, Intercalation, Electrode materials, Shuttling cations

1. Introduction

Excessive fossil fuel consumption under rapid economic development has caused a series of problems. First, the combustion of fossil fuels generates severe air pollution, such as small organic molecules, heavy metals, NO_x, and SO_2, in addition to acid rain derived from the latter two which causes further ecological effects [1]. Moreover, a considerable amount of carbon has existed on earth in the form of fossil fuels for millions of years. Therefore, massive emission of greenhouse gases from fossil fuels in a short time has broken the balance of the carbon cycle, leading to global temperature increase and other concomitant issues [2]. Finally, we must face a potential future depletion of fossil fuels with such a booming present consumption rate [3].

To find a way out of these dilemmas, researchers have directed their attention to the electricity collected from renewable energy sources including solar, wind, geothermal, tidal, and hydro. Despite significant development in recent years, the volatility,

Accepted manuscript

ACCEPTED MANUSCRIPT

intermittency and randomness of many renewable energy sources prevents them from fully replacing traditional fossil fuels [4]. Thus, an efficient GES is required to reconcile the imbalance between the irregularity of renewable energy and multifarious consumption of electricity. Distinct from the primary requirement of high energy density and high power density in portable electronics and electric vehicles, low cost, long cycling life, high safety, and high round-trip energy efficiency are the most critical parameters for GES [5]. Among mechanical energy storage systems, pumped hydro and compressed air suffer from location-dependent restrictions, enormous upfront costs and low energy efficiency, though the former provides the majority of energy storage on the current grid system [6, 7]. Flywheel energy storage is attractive due to its high power density and energy efficiency, but the high cost blocks its broad application [8]. Chemical energy storage systems rely on a combined electrolysis-fuel cell process, but H_2 storage complications, safety concerns, and high catalyst cost lower their competitiveness [9-11]. As for electric double layer capacitors and superconducting magnetic coils, which are two examples of electrical energy storage systems, the former is limited by its low output voltage, low energy density, and high self-discharge rate, while the latter with a quick response time and high round-trip efficiency is only practically used in high-energy physics experiments and nuclear fusion due to its high cost [12-14]. Compared with the above solutions, electrochemical energy storage has increasingly exhibited its unique virtues of low cost, high energy efficiency, high round-trip efficiency, long cycle life, controllable energy and power output in nascent yet promising battery energy storage systems [15-20].

Accepted manuscript

In contrast with nonaqueous electrochemical energy storage systems containing an expensive organic solvent with high toxicity and flammability, aqueous based electrochemical systems show competitive and distinct advantages in GES [21-23]. Lead-acid batteries and nickel metal hydride batteries are the most commonly employed aqueous rechargeable batteries. Lead-acid batteries are widely used in automotive systems for engine starting, lighting and ignition due to their low cost.

ACCEPTED MANUSCRIPT

However, the low capacity, limited cycle life, and poor energy efficiency render them unsuitable for GES [24, 25]. Nickel metal hydride batteries have been used for portable electronics and electric vehicles since 1990 and show some potential for GES. Nevertheless, problems such as the memory effect, low energy efficiency, and high cost remain mostly unsolved even after extensive work [26, 27].

In contrast with lead-acid batteries and nickel metal hydride batteries, intercalation based rocking-chair batteries are especially attractive for GES owing to their unique benefits. Among them, two primary benefits are stable cycling life and potentially high power density, besides the high energy density, high round-trip energy efficiency, and high safety [28-31]. Their stable cycling performance arises from reversible structure changes during intercalation reactions, which are entirely different from poor reversibility of phase transformations during the conversion reactions for lead-acid batteries and nickel metal hydride batteries. On the other side, their high power density originates from rapid ion diffusion pathways, including interlayers and channels, inside the intercalatable electrode structures. On the contrary, lead-acid batteries and nickel metal hydride batteries are deficient in such an intrinsic advantage due to their phase conversion reactions, leading to inferior rate performance.[32, 33]

Since the concept of aqueous Li-ion batteries (LIBs) introduced by Dahn *et al.* in 1994, aqueous Li-ion and Na-ion batteries (NIBs) have been well studied [34]. As shown in **Figure 1**, the stable voltage window of aqueous electrolytes is 1.23 V without considering the overpotential of hydrogen evolution reaction (HER) and oxygen evolution reaction (OER), which is much lower than the typical value of 3 V for nonaqueous electrolytes [35]. The narrow electrolyte window is one of the primary reasons why aqueous batteries always have lower energy density than the nonaqueous counterpart. Moreover, potential boundaries vary under different pH values. Thus, the stability of electrode materials should be considered when selecting different electrolytes. **Figure** 1 summarizes commonly used electrode materials for aqueous LIBs and NIBs, which are categorized into four types: oxides,

Accepted manuscript

polyanionic compounds, Prussian blue analogues and organic compounds [29]. In the first aqueous LIBs, an energy density of 75 Wh/Kg was delivered based on a set-up of $LiMn_2O_4$ as the cathode, VO_2 as the anode and $LiNO_3$ (5 mol/L) as the electrolyte. $Na_4Mn_9O_{18}$ was first proved to be a suitable electrode material for aqueous NIBs with a capacity of 45 mAh/g at a current density of 0.25 mA/g. Beyond this general introduction, systematic reviews of aqueous LIB and NIB electrode materials can be found elsewhere [29, 34].

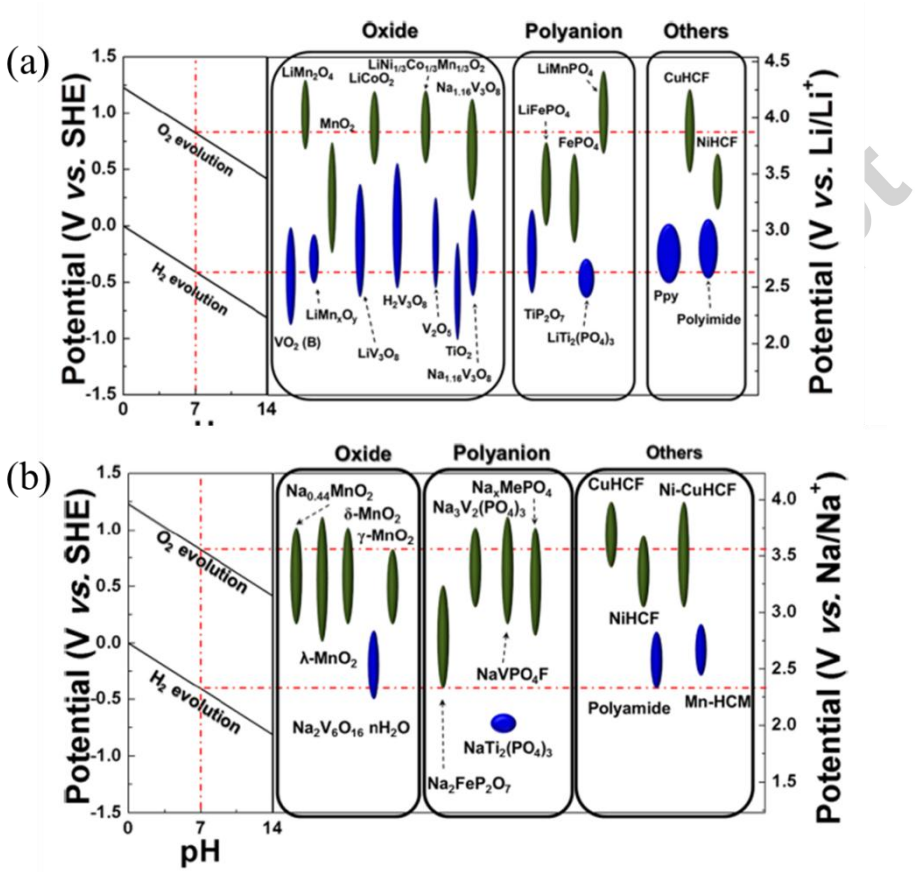

Figure 1 (a) Electrode materials for aqueous LIBs. (b) Electrode materials for aqueous NIBs. Reproduced with permission.[29] Copyright 2014, American Chemical Society.

Exploring novel intercalation chemistry not only has a significant influence on fundamentals, but also provides more choices of electrode materials with potentially higher capacity and better cyclability. Therefore, researchers have started to explore aqueous intercalation-type electrode materials with novel shuttling cations. As shown in **Figure 2**, the number of publications in this nascent field since 2015 has

ACCEPTED MANUSCRIPT

dramatically increased. The research area of aqueous intercalation-type electrode materials beyond those for Li-ion and Na-ion batteries will no doubt become a focal point as GES gain more widespread attention. Therefore, in this review paper, we summarize recent progress in this field with the purpose of providing a reliable basis and clear direction for future research.

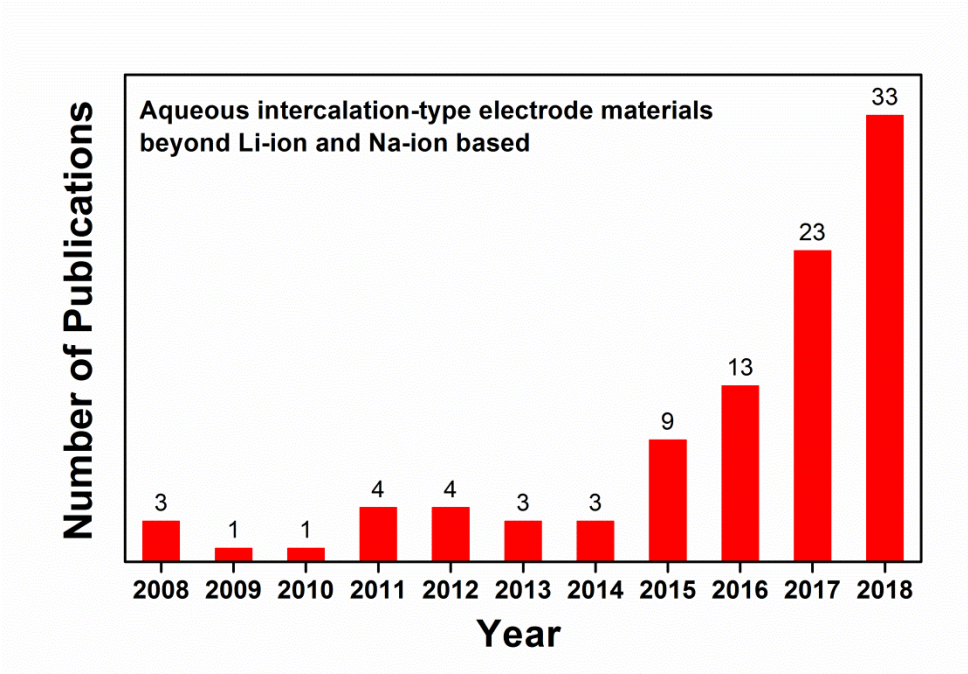

Figure 2 Number of publications for aqueous intercalation-type electrode materials beyond Li-ion and Na-ion based from January 2008 to May 2018.

This review paper focuses on cations other than Li^+ and Na^+, including NH_4^+, H_3O^+, K^+, Rb^+, Mg^{2+}, Zn^{2+}, Ca^{2+}, Sr^{2+}, Ba^{2+}, Cu^{2+}, Ni^{2+}, Pb^{2+}, Y^{3+}, La^{3+}, and Al^{3+}. Related electrode materials and their potential ranges are summarized in **Figure 3a**. After careful review, we find an apparent structural similarity between these materials, namely well-defined channels or interlayer spaces. Specifically, Prussian blue analogue, λ-MnO_2, todorokite MnO_2, α-MnO_2, γ-MnO_2, β-MnO_2, $ZnMn_2O_4$, $Zn_{0.25}V_2O_5{\cdot}nH_2O$, Anatase TiO_2, $Na_3V_2(PO_4)_3$ and MoO_3 are capable of storing cations by their suitable channel sizes, whereas graphite Birnessite MnO_2, perylene-3,4,9,10-tetracarboxylic dianhydride (PTCDA), VS_2, V_2O_5, 3,4,9,10-perylenetetracarboxylic diimide (PTCDI), Mxenes store cations within the

flexible layer structure. Thus, compounds containing interlayer spaces or channels, within stable aqueous electrolytes voltage window, should receive more attention in the search for novel electrode materials for aqueous intercalation-type batteries.

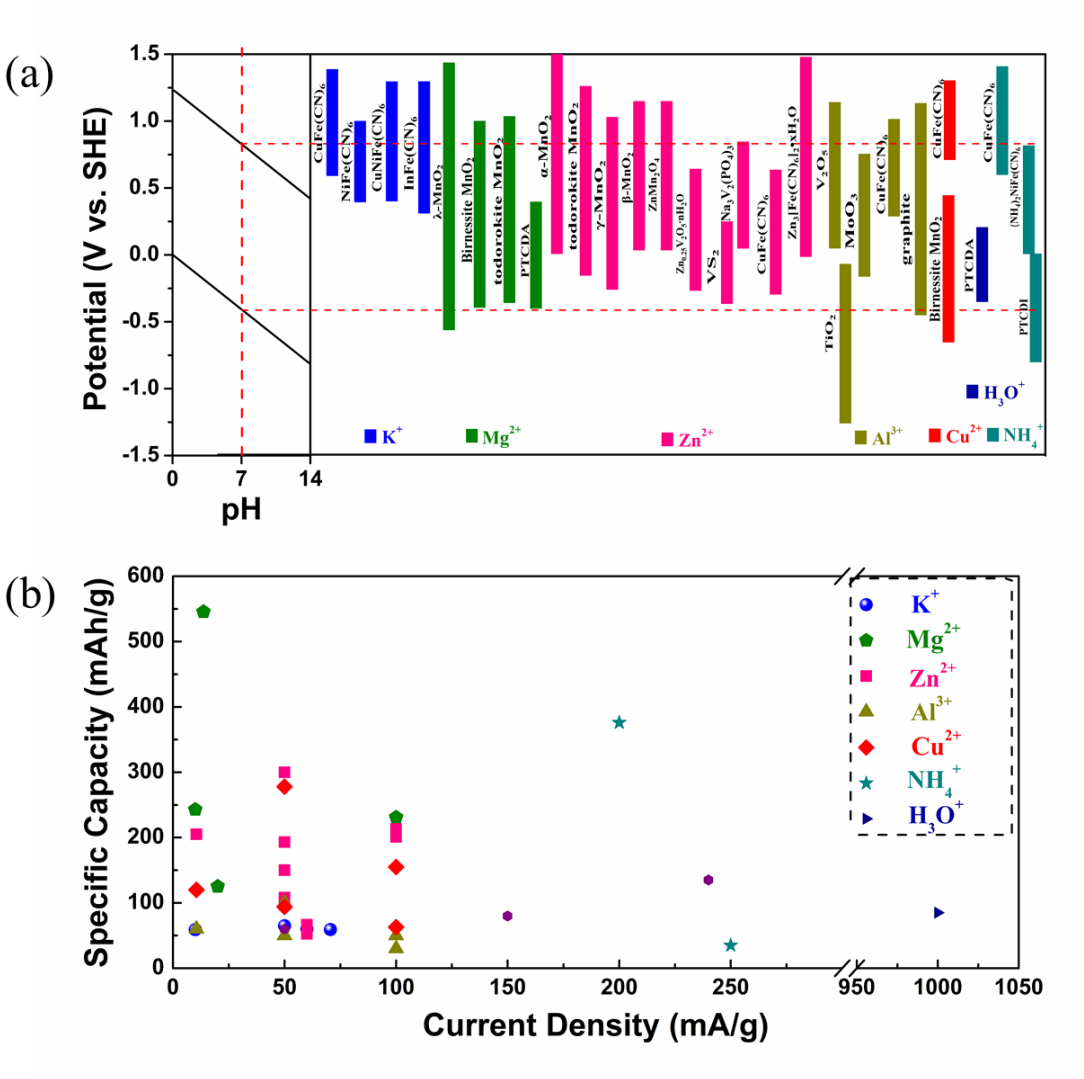

Figure 3 (a) Aqueous intercalation-type electrode materials beyond Li-ion based and Na-ion based (b) Corresponding capacity at specific current density.

Capacities at specific current density for these electrode materials are summarized in **Figure 3b,** and specific values are listed in **Table 1**. Typical capacities for these electrode materials are between 50-200 mAh/g with a corresponding current density between 50-100 mA/g. If we consider an aqueous battery voltage of 1 V, then the typical energy density is between 50-200 Wh/kg with a power density in the range of 50-200 W/kg. It should be noted that the calculated energy density and power

ACCEPTED MANUSCRIPT

density are based on the single electrode material, without considering the counter electrode, electrolyte, and other battery components. In terms of practical applications as a full cell, the most promising type of aqueous rocking-chair batteries should be Zn^{2+} based if considering a meaningful battery operating voltage. Specifically, Zn metal can be directly used as a stable anode providing sufficient shuttling cations in the aqueous electrolyte. Nevertheless, other types of aqueous rocking-chair batteries lack of this superiority due to the absence of capable anodes.

Table 1 Summary of aqueous intercalation-type electrode materials beyond Li-ion and Na-ion based and their electrochemical performance.

Inserted Ions	Material	Current Density (mA/g)	Capacity (mAh/g)	Capacity Retention	
K^+	$CuFe(CN)_6$	70.55	59.14	83%@40000th cycle	Ref [36]
	$NiFe(CN)_6$	10	59	93%@5000th cycle	Ref [37]
	$CuNi(CN)_6$	50	65	91%@2000th cycle	Ref [38]
	$InFe(CN)_6$	60	60	NA	Ref [39]
Mg^{2+}	λ-MnO_2	13.6	545.6	70%@50th cycle	Ref [40]
	Birnessite MnO_2	100	231	62.5%@10000th cycle	Ref [41]
	Todorokite MnO_2	10	243	83.7%@300th cycle	Ref [42]
	PTCDA	20	125	NA	Ref [43]
Zn^{2+}	α-MnO_2	10.5	205	62%@30th cycle	Ref [44]
	Todorokite MnO_2	50	108	97%@50th cycle	Ref [45]
	γ-MnO_2	100	201	63%@40th cycle	Ref [46]
	β-MnO_2	100	213	NA	Ref [47]
	$ZnMn_2O_4$	50	150	94%@500th cycle	Ref [48]
	$Zn_{0.25}V_2O_5{\cdot}nH_2O$	50	300	80%@1000th cycle	Ref [49]
	VS_2	50	193	98%@200th cycle	Ref [50]
	$Na_3V_2(PO_4)_3$	50	97	74%@100th cycle	Ref [51]
	$CuFe(CN)_6$	60	52.5	96%@100th cycle	Ref [52]
	$Zn_3[Fe(CN)_6]_2$	60	66.5	86%@100th cycle	Ref [53]
Al^{3+}	V_2O_5	60	120	58%@12th cycle	Ref [54]
	TiO_2	50	278.1	140%@14th cycle	Ref [55]
	MoO_3	30	155	93%@1800th cycle	Ref [56]
	$CuFe(CN)_6$	50	62.9	54.9%@1000th cycle	Ref [57]
Cu^{2+}	Graphite	100	94	94%@200th cycle	Ref [58]
	Birnessite MnO_2	200	376	80%@1000th cycle	Ref [59]
H_3O^+	$CuFe(CN)_6$	250	35	NA	Ref [60]
	PTCDA	1000	85	70%@120th cycle	Ref [61]
NH_4^+	$CuFe(CN)_6$	50	60	91%@500th cycle	Ref [62]
	$(NH_4)_2NiFe(CN)_6$	150	80	74%@2000th cycle	Ref [63]

Accepted manuscript

ACCEPTED MANUSCRIPT

PTCDI	240	135	89.5%@400th cycle	Ref [63]

2. K^+ based intercalation-type electrode materials

Prussian blue analogues have a perovskite-type structure with a general formula $A_xB[Fe(CN)_6]_y \cdot mH_2O$. Here, A stands for an alkali metal, B stands for a transition metal, and the value of x and y fall into the range of $0 \leq x \leq 2$ and $y < 1$, respectively. Iron and transition metal atoms are connected by cyanide groups, and the alkali metal sites are always used for cation intercalation. The intercalation behavior of K^+ into Prussian blue, $KFe^{3+}Fe^{2+}(CN)_6$, was first investigated by Neff *et al.* in 1978 [64-67]. Impurity from the insoluble nature of Prussian blue resulted in poor performance at that time, but battery performance was improved by Wang *et al*. later on [68].

In 2011, Cui *et al.* synthesized $KCuFe(CN)_6$ with high crystallinity by a controlled co-precipitation method [36]. The S shape curve from cyclic voltammetry in 1 M KNO_3 and 0.01 M HNO_3 electrolyte suggested a solid solution reaction mechanism during K^+ intercalation and deintercalation. The theoretical capacity was around 85 mAh/g; however, the observed value in this work was only 60 mAh/g at a current density of 0.83 C due to the existing zeolitic water and nonstoichiometry of the compound. Moreover, 40 mAh/g could be maintained even at a high current density of 83 C. This is a benefit of the open structure, which was further proved by the fact that the kinetic limiting factor was electrolyte resistance rather than charge transfer inside the crystal lattice. The cycling performance was also remarkable with 83 % capacity retention after 40000 cycles, attributed to the one phase reaction mechanism with only 0.9% isotropic lattice parameter fluctuation during the charge/discharge process [69].

Following the research of a nickel hexacyanoferrate thin film as an electrode material, the same group investigated electrochemical performance of nickel hexacyanoferrate

Accepted manuscript

ACCEPTED MANUSCRIPT

at a high mass loading of 10 mg/cm^2 [37, 70, 71]. The as-synthesized nickel hexacyanoferrate by precipitation delivered a reversible capacity of 60 mAh/g at a current density of 10 mA/g, and superior rate capability and cycling performance, comparable to the copper hexacyanoferrate mentioned above. Later on, the authors further proved copper-nickel alloy hexacyanoferrate nanoparticles as a remarkable host for K^+ intercalation [38].

Besides studying the electrochemical performance of indium hexacyanoferrate as aforementioned Prussian blue analogues, Liu *et al*. also revealed detailed intercalation mechanisms [39]. The authors found that bare K^+ was solely inserted into the interspace of indium hexacyanoferrate whereas Li^+ and Na^+ were co-inserted with a water molecule, which was due to different ionic sizes. Without co-insertion with water, K^+ intercalation showed a lower overpotential and increased diffusion kinetics than that of Li^+ and Na^+ with water co-insertion, which had never been noticed before. It should be noted here this phenomenon also occurred in copper hexacyanoferrate [72].

Compared with intensive investigations in K^+ based cathode materials, exploration of potential K^+ based anode materials is sparse [73, 74]. Only MoO_3 have been studied to date. As reported by Park *et al.*, K^+ was inserted into the interlayer of MoO_3 with its lattice parameters increased, which further induced surface cracks and anisotropic electrode swelling. The above structural instability was suggested as the reason for the decayed cycling performance [75]. However, the severe capacity fading calls for a detailed study of the mechanism behind the potassiation and depotassiation, which should shed light on a rational structural design that could be employed to improve the electrochemical performance.

3. Mg^{2+} based intercalation-type electrode materials

The initial work on Mg ion batteries focusing on Mg^{2+} intercalation into transition metal oxides and transition metal sulfides in organic electrolyte was investigated by

Accepted manuscript

ACCEPTED MANUSCRIPT

Winterton in 1990 [76]. Later on, Desilvestro *et al.* found that H_2O solvated Mg^{2+} can be inserted into V_2O_5 with capacity up to 170 mAh/g in acetonitrile containing 1M $Mg(ClO_4)_2$ and 1M H_2O [77]. In contrast with tremendous efforts put into nonaqueous Mg-ion batteries, the study of Mg-ion batteries in aqueous electrolytes is still in its infancy; only a few cathode materials have been investigated, such as MnO_2, V_2O_5, Prussian blue analogues, poly(dioxyethane thiophene) (PEDOT), PTCDA and so on. [28, 40-43, 78-93].

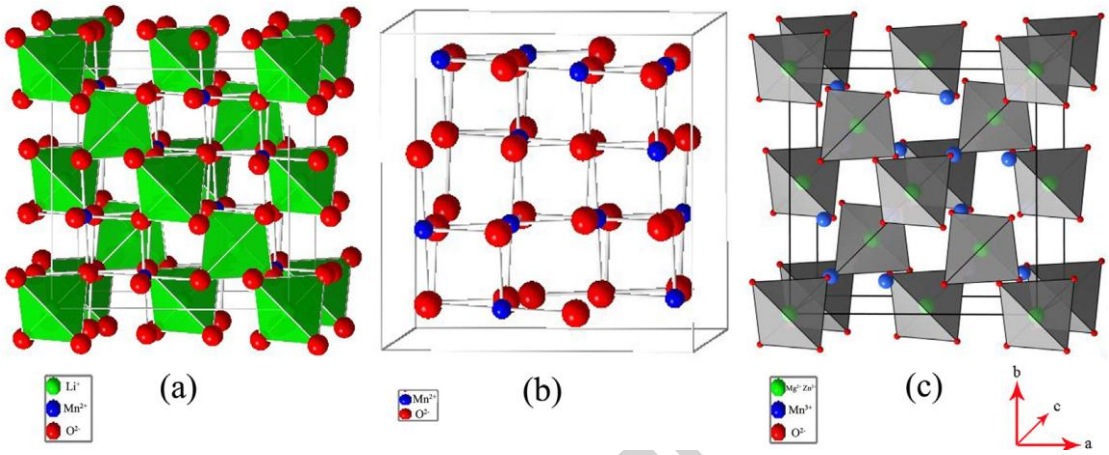

Figure 4 (a) Crystal structure of $LiMn_2O_4$ (b) λ-$MnO_2$with void spaces after the removal of Li^+ (c) MMn_2O_4(M = Mg, Zn) after the intercalation of M^{2+}. Reproduced with permission.[40] Copyright 2014, Elsevier.

Vuorilehto *et al*. first studied MnO_2 as a cathode for aqueous Mg-ion batteries with an energy density of 87 Wh/kg at a power density of 15 W/kg in 2002 [87]. This work mainly investigated the voltage loss, heat evolution, and environmental impact during the operation of the battery. However, a detailed mechanism of structural changes during the electrochemical reactions was not advanced until 2013. As reported by Cao *et al.*, λ-MnO_2 was synthesized from leaching $Li_2Mn_2O_4$ with dilute H_2SO_4, with structural changes during this process shown in **Figure 4** [40]. With the intercalation of Mg^{2+}, as-formed $MgMn_2O_4$ maintained its spinel structure, and the oxidation state of Mn decreased from 4+ to 3+. The discharge capacity was as high as 545.6 mAh/g in the $MgCl_2$ electrolyte under a current density of 13.6 mA/g.

ACCEPTED MANUSCRIPT

Besides λ-MnO_2, a Mg octahedral molecular sieve composed of the discharged state of todorokite-type MnO_2 was also studied as the cathode material for an aqueous Mg-ion battery recently [42]. As shown in **Figure 5**, the basic structure of MnO_6 consists of a panel connected by edge-sharing; then four panels form a 3× 3 tunnel by the corner sharing of MnO_6. The whole channel was propped up by Mg^{2+} and corresponding water molecules during the charging process. Later on, the same group further investigated a Mg octahedral molecular sieve with the 2× 2 tunnel [86].

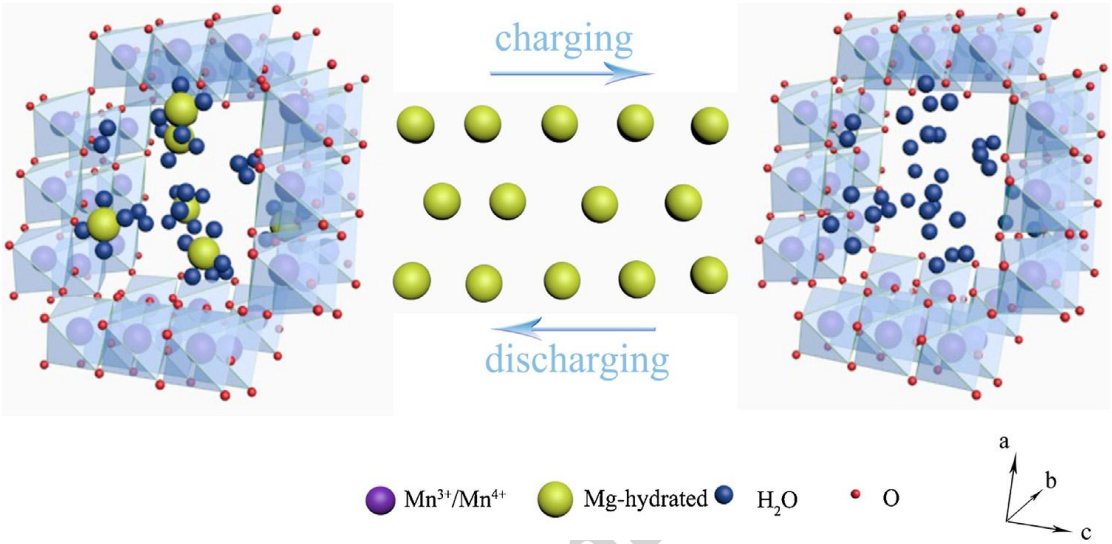

Figure 5 A schematic illustration of the insertion/deinsertion process of Mg^{2+} ions in an aqueous system. Reproduced with permission.[42] Copyright 2017, Elsevier.

Like organic electrolytes in nonaqueous batteries, the solvation energy of cations affects the electrochemical performance dramatically. In a study of todorokite-type MnO_2 as a Mg^{2+}-intercalation type cathode under different aqueous electrolytes, the authors found that Mg octahedral molecular sieve showed better capacity, rate capability, and cycling stability in $MgCl_2$ and $Mg(NO_3)_2$ electrolyte than those in the $MgSO_4$ electrolyte. The electrolyte influence could be explained by the negative Jones–Dole coefficient for Cl^- and NO_3^- which was positive for SO_4^{2-}. Easier desolvation of Mg^{2+} in $MgCl_2$ and $Mg(NO_3)_2$ electrolyte provided easy access for insertion and extraction [85].

Compared with the composition of different aqueous electrolytes, crystal water inside

ACCEPTED MANUSCRIPT

the structure holds a more important role in the intercalation-deintercalation process. Layered Birnessite MnO_2 containing crystal water was synthesized out of spinel-Mn_3O_4 by the electrochemical method [41]. With corner-shared Mn^{2+} diffused out of the structure, edge-shared Mn^{3+} was oxidized into Mn^{4+}, and crystal water was inserted at the same time. The layer distance also increased from 4.97 Å to 7.25Å during this process. The crystal water was indispensable in maintaining the layer structure; otherwise, the layered structure went back to the spinel structure after heat treatment. Based on annular bright field results, the authors revealed Mg^{2+} was inserted into Mn layers, mixing with Mn atoms, rather than intercalated into the interlayer of MnO_2. This phenomenon was very rare for the layered material used as an intercalation host. More surprisingly, three desolvated H_2O molecules from Mg^{2+} were co-intercalated in the discharge process based on the TGA result. As shown in **Figure 6,** a water layer formed between MnO_2 layers by the rearrangement of inserted water molecules and the original crystal water molecule. Here, it should be noted that the crystal water inside the structure not only stabilized the layer structure but also took part in forming an interacting water layer at the end of the discharge process. Moreover, the shielding effect from the crystal water for Mg^{2+} and negative host considerably decreased the overpotential and increased the rate capability.

Figure 6 A graphical illustration of the insertion of hydrated Mg^{2+} and Mg/Mn mixing during the discharge process. Reproduced with permission.[41] Copyright 2015, American Chemical Society.

The work mentioned above pointed out that crystal water inside the structure and desolvated water from Mg^{2+} influence the intercalation and deintercalation behavior

ACCEPTED MANUSCRIPT

of Mg^{2+} inside the MnO_2 crystal lattice. However, this view has been recently challenged by Cabana *et al.* [84]. Starting with fully delithiated Li_2MnO_4 by acid leaching and electrochemical charging, the authors concluded that Mg^{2+} could be reversibly inserted and extracted from the Mn_2O_4 framework without H_2O participation in the aqueous electrolyte, which was further confirmed by the formation of $MgMn_2O_4$ in a nonaqueous electrolyte. Due to the contradicting accounts, it is difficult to determine the real process of the Mg^{2+} intercalation into the spinel manganese oxide. Therefore, a systematic and thorough study is required in the future.

Unlike the rigid structure of metal oxides or Prussian blue analogues with strong ionic bonding, the flexible interlayer space assembled by weak van der Waals' forces in organic solids seems more likely to facilitate an easier Mg^{2+} intercalation and deintercalation. Recently, organic solid PTCDA was studied as a cathode for Mg-ion batteries by Ji *et al.* [43]. Based on the *ex situ* X-ray diffraction (XRD) and transmission electron microscopy (TEM) results, the authors found (011) layer spacing decreased while (021) layer spacing increased during the Mg^{2+} insertion process. Further investigation by first principle calculation revealed that the above phenomenon originated from the rotation of three adjacent PTCDA columns when hosting a Mg^{2+} cation. A reversible capacity of 125 mAh/g was obtained in a three-electrode cell set-up.

4. Zn^{2+} based intercalation-type electrode materials

Compared with other aqueous ion batteries, Zn-ion rechargeable aqueous batteries are especially attractive due to the following advantages of a Zn anode: the lower price resulting from its wide distribution and well-established industrial production, the nearly 2V electrolyte window derived from its high overpotential for HER, and relatively minor dendrite formation under neutral pH condition. However, cathode materials with remarkable Zn intercalation performance are still lacking. Up to now,

Accepted manuscript

ACCEPTED MANUSCRIPT

MnO_2, VS_2, Prussian blue analogue, $Na_3V_2(PO_4)_3$, zinc metal oxide and other compounds have been investigated [44-47, 94-123].

α-MnO_2 was first studied as a cathode material for Zn-MnO_2 secondary batteries in $ZnSO_4$ electrolyte by Kang *et al.*, even though Zn-MnO_2 primary batteries in KOH electrolyte have already been widely used since 1860 and dominate the primary battery market [100]. For the Zn-MnO_2 primary battery, the first step of the electrochemical reaction is typically presented as follows:

Cathode: $MnO_2 + H_2O + e^- \rightarrow MnOOH + OH^-$

Anode: $Zn + 4OH^- \rightarrow [Zn(OH)_4]^{2-} + 2e^-$

With further discharge, the second step of the electrochemical reaction is presented as follows:

Cathode: $MnOOH + H_2O + e^- \rightarrow Mn(OH)_2 + OH^-$

Anode: $Zn + 2OH^- \rightarrow Zn(OH)_2 + 2e^-$

However, the electrochemical reactions for Zn-MnO_2 secondary batteries were described differently by the authors, even though the open circuit voltages of both were similar:

Cathode: $2MnO_2 + Zn^{2+} + 2e^- \rightarrow ZnMn_2O_4$

Anode: $Zn \rightarrow Zn^{2+} + 2e^-$

The electrochemical reactions for Zn-MnO_2 primary batteries are irreversible, especially when discharged beyond the second step, but Zn^{2+} could be reversibly inserted in or extracted from the channels of MnO_2 in a Zn-MnO_2 secondary battery. When the Zn-MnO_2 secondary battery was discharged at 0.5 C, the capacity was about 210 mAh/g, much higher than 125 mAh/g for Zn-MnO_2 primary batteries.

Accepted manuscript

ACCEPTED MANUSCRIPT

After 100 cycles, the capacity of the Zn-MnO_2 secondary battery dropped from 130 mAh/g to 100 mAh/g.

The mechanism of Zn^{2+} intercalation into α-MnO_2 was not fully revealed in this work, though the intercalation phenomenon had been confirmed by XRD and X-ray photoelectron spectroscopy (XPS) results. It was Lee *et al.* who further clarified the structural transformations of MnO_2 between the tunneled phase and the layered birnessite-like phase shown in **Figure 7** by *ex situ* XRD and selected area electron diffraction (SAED) [44]. The XAS results indicated that the Mn oxidation state increased during the discharge process, but this result was against the prevailing notion that the oxidation state of Mn should decrease with injected electrons from the anode side. The authors ascribed the contradiction to Mn^{2+} dissolution into the electrolyte with the Mn vacancies formed, during which the oxidation state of remaining Mn increased. Dissolved Mn^{2+} would return to the host by combining with the vacancies in the charging process. Based on the above results, the authors concluded that Mn could hold a high oxidation state in the whole discharge and charge process by the dissolution and retrieval of Mn^{2+}.

Later on, the authors corrected themselves by stating that layered Zn-buserite was the discharged product, rather than layered birnessite, based on the loss of intercalated Zn^{2+} and the surrounding water molecules [99]. The authors also pointed out that the capacity fading was due to the structural strain, especially the channel volume changes during the phase transition between tunneled α-MnO_2 and layered Zn-buserite. Therefore, a suitable cathode host with stable cycling performance should have a larger channel volume, such as todorokite (3× 3 channel size), rather than α-MnO_2 (2× 2 channel size). This conjecture was demonstrated subsequently [45].

Accepted manuscript

ACCEPTED MANUSCRIPT

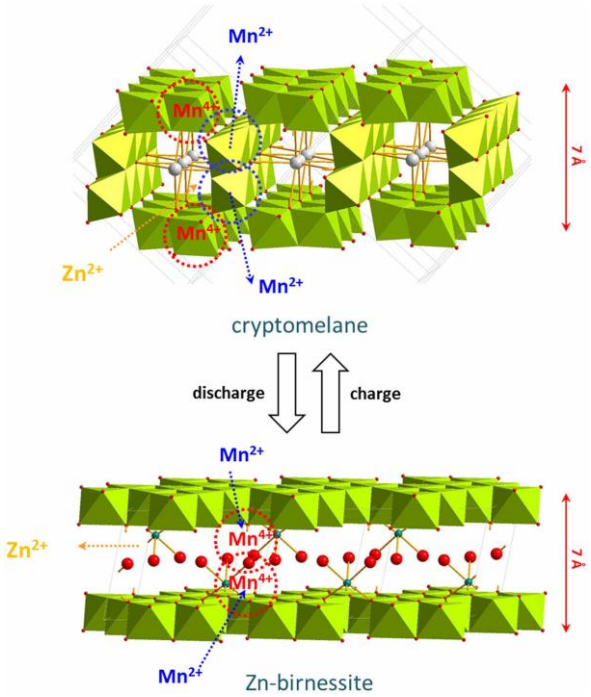

Figure 7 Schematic illustrating the mechanism of zinc intercalation into α-MnO_2. Reproduced with permission.[44] Copyright 2014, Springer Nature.

Further investigating the electrochemical mechanism for a Zn-α-MnO_2 secondary battery, Liu *et al.* offered a different opinion [98]. Firstly, the dissolved Mn^{2+} in the discharge process could never be retrieved in the charging process. A continuing loss of Mn^{2+} was the reason for capacity fading until the solution equilibrium was established, further proved by the improved cycling performance after $MnSO_4$ was added. Secondly, real capacity came from the conversion reaction between protons and MnO_2, rather than intercalation of Zn^{2+} into MnO_2. This concept treated the cathode electrochemical reaction of the Zn-α-MnO_2 secondary battery the same as that of the Zn-MnO_2 primary battery. The only difference between Zn-MnO_2 secondary batteries and Zn-MnO_2 primary batteries lay in the reversibility of product formed at Zn electrode under different pH conditions. To summarize, researchers put forward two contradictory reaction pathways for the Zn-α-MnO_2 secondary battery, both of which seem to be plausible. Whether conversion reaction or intercalation reaction takes place in the Zn-α-MnO_2 secondary battery requires further investigation.

Accepted manuscript

ACCEPTED MANUSCRIPT

Compared with a size of 4.6 Å in the 2×2 channels for α-MnO_2 and a size of 7.0 Å in 3×3 channels for todorokite-type MnO_2, the channel size of γ-MnO_2 is much smaller, only 1×1 for pyrolusite or 1×2 for ramsdellite, which therefore seems unsuitable for cathode materials based on the conclusion mentioned above. However, Kim *et al*. demonstrated that the unique γ-MnO_2 structural changes during electrochemical reaction still made it applicable as a cathode material for Zn-ion secondary batteries [46]. Based on the *in situ* X-ray absorption near edge spectroscopy (XANES) and synchrotron XRD results, the authors found that partial tunnel-type γ-MnO_2 converted into spinel-type $ZnMn_2O_4$ in the early stage of discharge with the oxidation state of Mn^{4+} decreasing to Mn^{3+}. However, the remaining tunnel-type γ-MnO_2 transformed into tunnel-type γ-$Zn_xMn_2O_2$ with further discharge. Finally, the coexistence of spinel-type $ZnMn_2O_4$, tunnel-type γ-$Zn_xMn_2O_4$, and layer-type Zn_yMnO_2 was detected in the discharge product shown in **Figure 8**. In the subsequent charge process, the discharge products could be oxidized back to γ-MnO_2.

Accepted manuscript

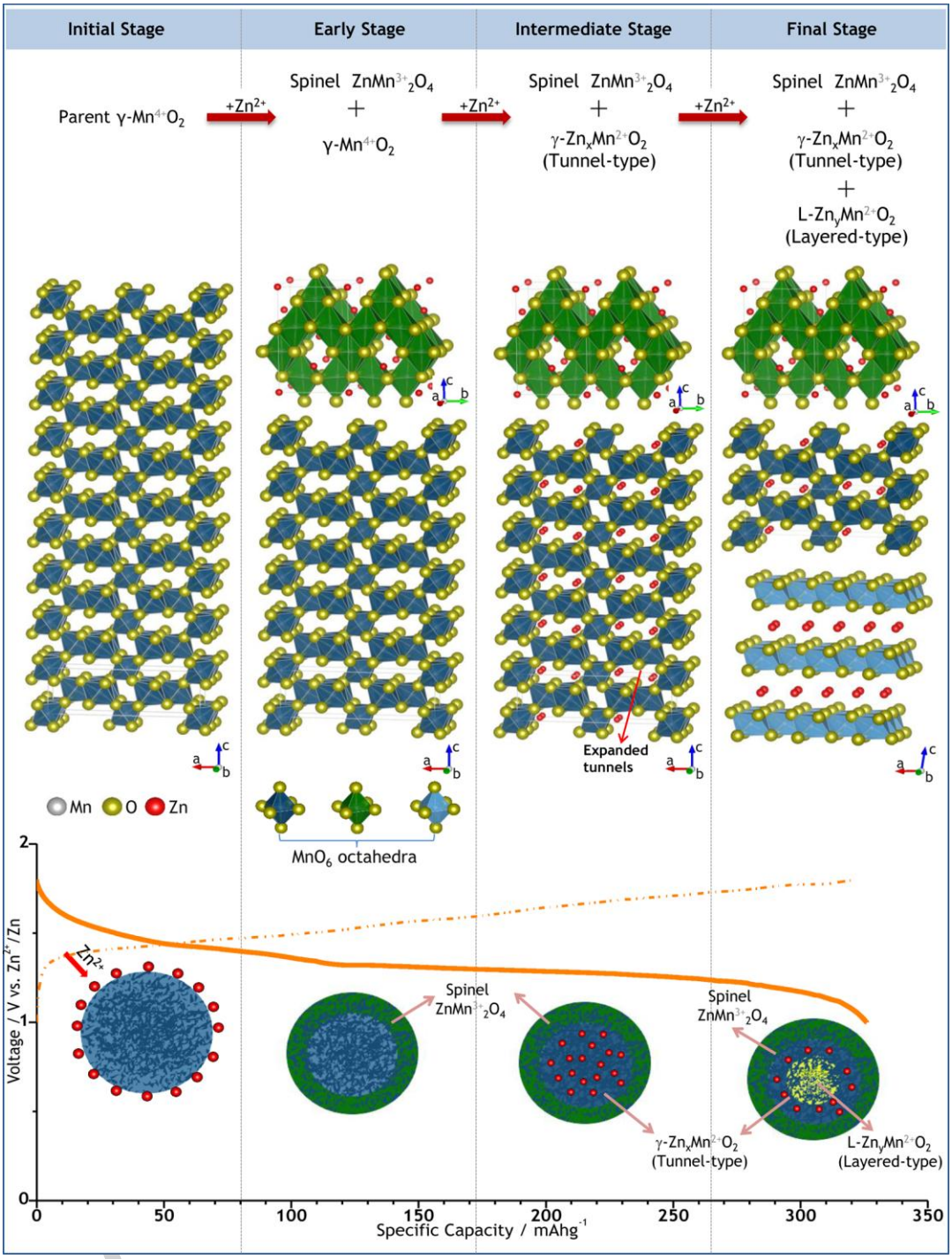

Figure 8 Schematic illustration of the reaction pathway of Zn-insertion in the prepared γ-MnO_2 cathode. Reproduced with permission.[46] Copyright 2015, American Chemical Society.

Similar to γ-MnO_2, the limited 1× 1 channel size of β-MnO_2 implies an unfavorable Zn^{2+} intercalation with a capacity of only about 58 mAh/g in aqueous $ZnSO_4$

electrolyte as reported by Kang *et al.* [47]. However, a reversible capacity as high as 225 mAh/g and a stable cycling performance of 94 % capacity retention after 2000 cycles were obtained by employing aqueous $Zn(CF_3SO_3)_2$ electrolyte [97]. As shown in **Figure 9,** the authors revealed that tunnel-type β-MnO_2 firstly transformed into layer-type Zn-buserite irreversibly, in and out of which Zn^{2+} was inserted and extracted in the subsequent cycles. In addition, the cathode integrity was enhanced by forming a porous MnO_2 layer on the surface of β-MnO_2.

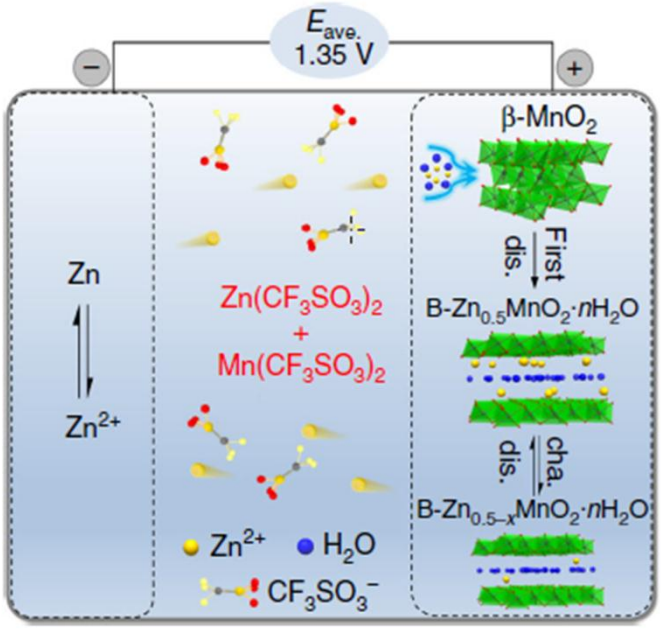

Figure 9 the rechargeable Zn-MnO_2 cell using $CF_3SO_3^-$-based electrolyte. Reproduced with permission.[97] Copyright 2017, Springer Nature.

Considering the improved LIB electrochemical performance by the successful succession from MnO_2 to $LiMn_2O_4$, $ZnMn_2O_4$ seems to be a promising cathode material for Zn-ion batteries. However, the high electrostatic repulsion among the Zn^{2+} cations within the channels prevents the intercalation of Zn^{2+} into $ZnMn_2O_4$. Recently, Chen *et al*. reported cation-defective $ZnMn_2O_4$ as a cathode material with a reversible capacity around 150 mAh/g at 50 mA/g, shown in **Figure 10a** [48]. According to the *ex situ* XRD in **Figure 10b** carried out at different stages of the Zn^{2+} intercalation/deintercalation, only peaks for spinel structure were observed, indicating that no phase transition occurred. The shift of XRD peaks corresponded to the

insertion or extraction of Zn^{2+}, in line with the intensity changes of Raman bands in **Figure 10c**. The valence state changes of Mn were observed by the peak changes in the synchrotron soft X-ray absorption spectroscopies in **Figure 10d**. All the results above demonstrated that the stable cycling of cation-defective $ZnMn_2O_4$ was due to the lack of phase transition during the charge/discharge process.

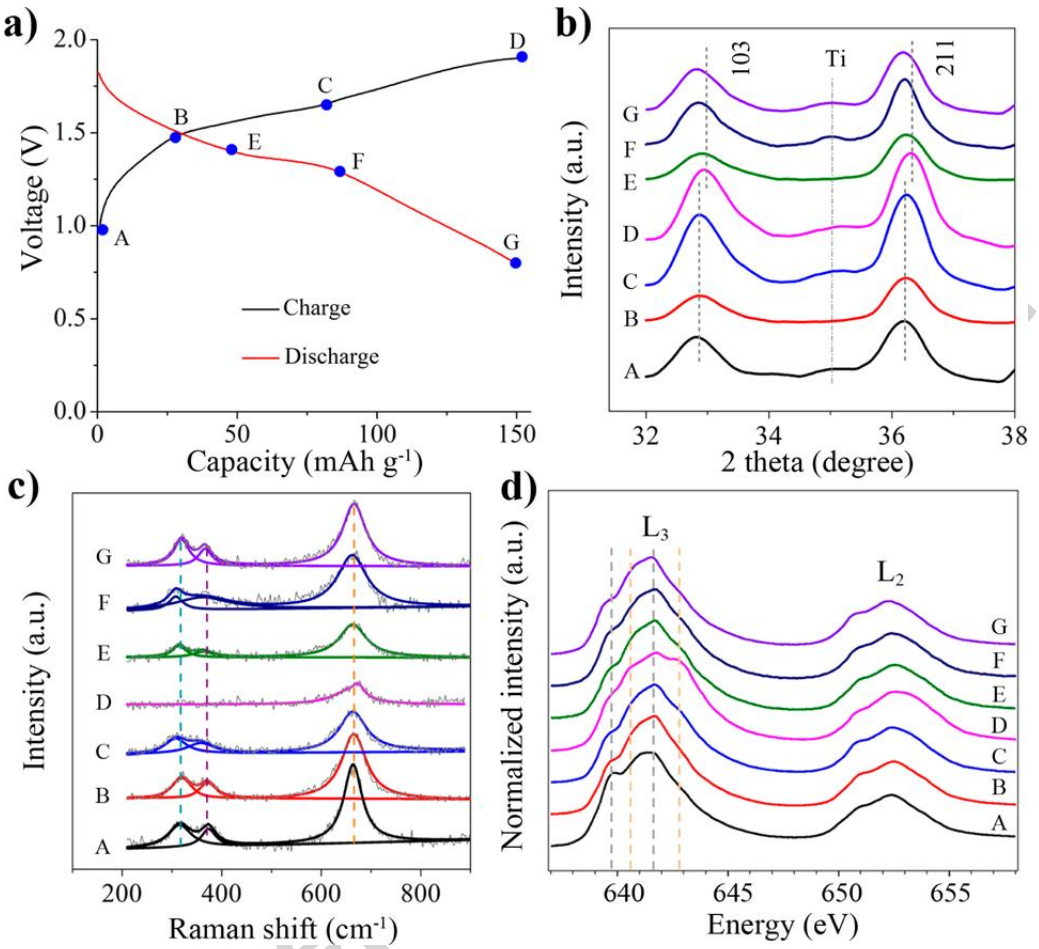

Figure 10. (a) Charge/discharge curves (third cycle) of ZMO/C electrode at 50 mA g−1 in 3 M $Zn(CF_3SO_3)_2$ electrolyte. The points marked the states where data were collected for analysis. (b) XRD patterns within selected angle (2θ) of 30−38°. (c) Raman spectra (gray curves) and Lorentzian fitting (colored solid profiles) in the wavenumber range of 200−900 cm−1. (d) SXAS of Mn L-edge spectra. Reproduced with permission.[48] Copyright 2016, American Chemical Society.

Beyond the intensive study of tunnel MnO_2, Huang *et al.* developed $Na_3V_2(PO_4)_3$ with sodium (Na) super ionic conductor (NASICON)-type structure as cathode material for

Zn-ion secondary batteries [51]. In the first charge process, two sodium cations were extracted from site 18e while only one sodium cation remained at site 6b. The formed $NaV_2(PO_4)_3$ confirmed by *ex situ* XRD provided an open site for Zn^{2+} intercalation as shown in **Figure 11**. In the subsequent discharge process, newly formed peaks were assigned to Zn^{2+}-intercalated NASICON structure. Rietveld-refined XRD patterns indicated Zn^{2+} cations not only occupied site 18e from original sodium position but also took site 6b, further proved by the uniform Zn distribution over the whole structure, rather than merely surface accumulation.

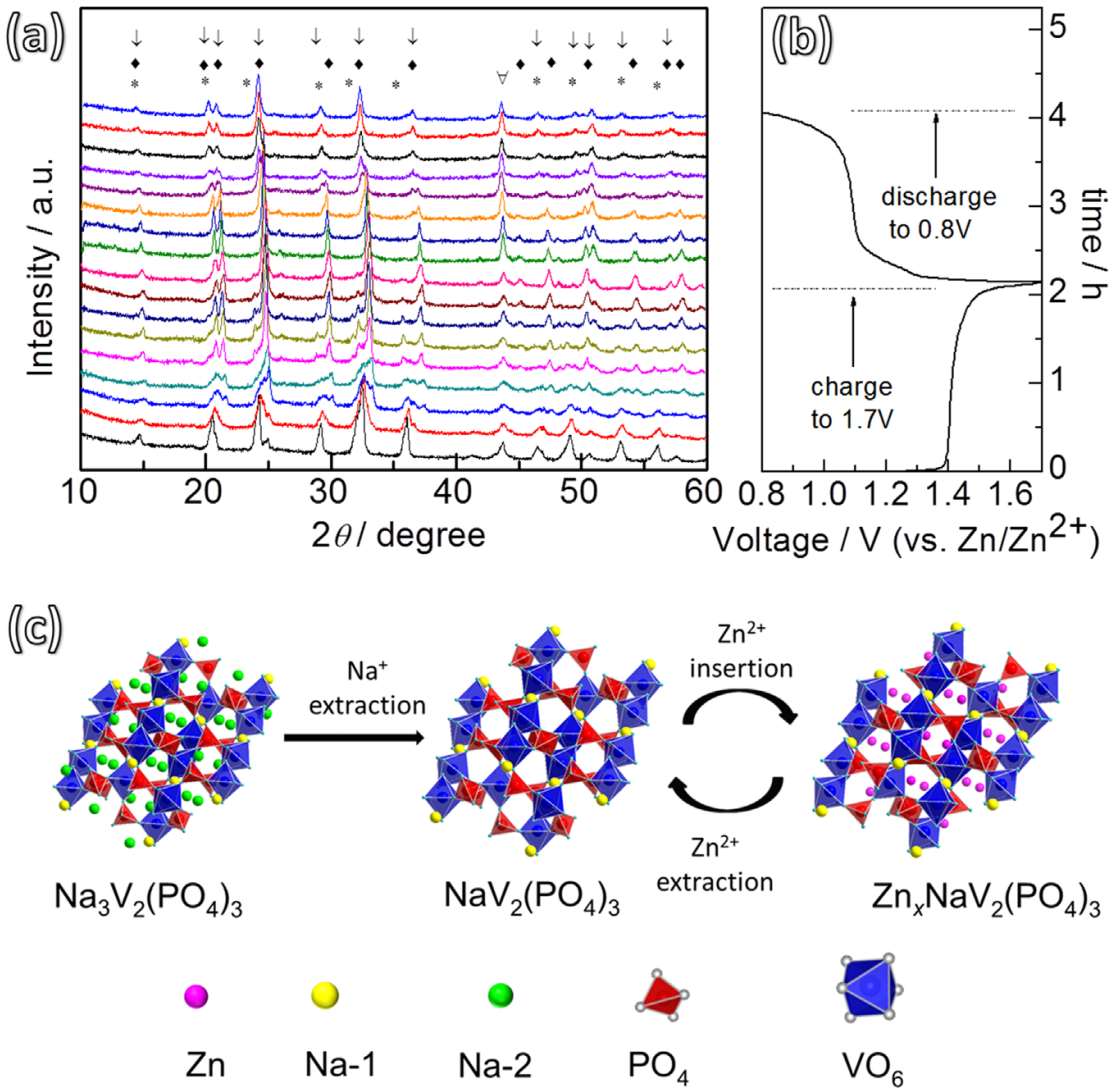

Figure 11 (a) Ex-situ XRD patterns of $Na_3V_2(PO_4)_3$ cathode for Zn-ion battery during the charge/discharge in a voltage of 0.8 – 1.7V, *$Na_3V_2(PO_4)3$, ♦ $NaV_2(PO_4)_3$, ↓ $Zn_xNaV_2(PO_4)_3$, ∀ stainless steel. (b) Corresponding voltage-time curves. (c) Schematic representation of phase transition of $Na_3V_2(PO_4)_3$ cathode during cycling.

ACCEPTED MANUSCRIPT

Reproduced with permission.[51] Copyright 2016, Elsevier.

Compared with the limited channel sizes of MnO_2, $ZnMn_2O_4$ and NASICON structure, the open-framework structure of Prussian blue analogues seems more attractive, especially for a superior rate performance. Copper hexacyanoferrate was proposed as cathode material for aqueous Zn-ion batteries by Mantia *et al.* [52]. Interestingly, the redox peak of Zn^{2+} intercalation or deintercalation was split into two peaks, which may be due to the strong electric repulsion between the metal cation in the host and Zn^{2+}. Almost at the same time, copper hexacyanoferrate was also investigated by Wang *et al.*, who concluded the solid phase diffusion controlled the intercalation/deintercalation of Zn^{2+} [124].

Unlike conventional Prussian blue analogues with cubic structure, zinc hexacyanoferrate possesses a rhombohedral structure [125]. Common dissolution phenomena of electrode materials did not happen in the zinc hexacyanoferrate case, implying a highly stable cycle life. Later, the same group developed cubooctahedral, truncated octahedral or octahedral structure by adjusting the dripping speed in the co-precipitation process. The subsequent electrochemical test revealed zinc hexacyanoferrate with cubooctahedral structure had a better rate capability and cyclic stability than the other two shapes due to the exposition of different facets [53].

Beyond the channel-type materials as we mentioned above, layer-type materials are the other big family of intercalable hosts. Recently, Nazar *et al.* reported a single-crystal $Zn_{0.25}V_2O_5{\cdot}nH_2O$ nanobelt as a Zn-ion battery cathode material with high specific capacity and long-term cycle stability [49]. The structure of as-prepared $Zn_{0.25}V_2O_5{\cdot}nH_2O$ is shown in **Figure 12**, with two-dimensional V_2O_5 double-sheets as the framework and ZnO_6 octahedra as interlayer pillars. When immersing in the electrolyte, $Zn_{0.25}V_2O_5{\cdot}nH_2O$ transformed into $Zn_{0.25}V_2O_5{\cdot}yH_2O$ spontaneously after H_2O molecules intercalating into the structure, forming H_2O double layers with an interlayer distance of 2.1Å. During cycling, water was

Accepted manuscript

ACCEPTED MANUSCRIPT

repelled out with Zn^{2+} intercalating into $Zn_{0.25}V_2O_5 \cdot yH_2O$ in the discharge process, and a reverse process happened during the charging process. The sloping curve in the galvanostatic test suggested Zn^{2+} intercalation/deintercalation was a solid solution process. Furthermore, XRD results revealed this process consisted of two regimes with different reaction mechanisms. In the first regime, d-spacing experienced a small contraction due to the decreased electrostatic repulsion of V_2O_5 layers when 0.3 Zn was inserted. In the second regime, d-spacing decreased dramatically due to further the increased screening effect with H_2O deintercalation.

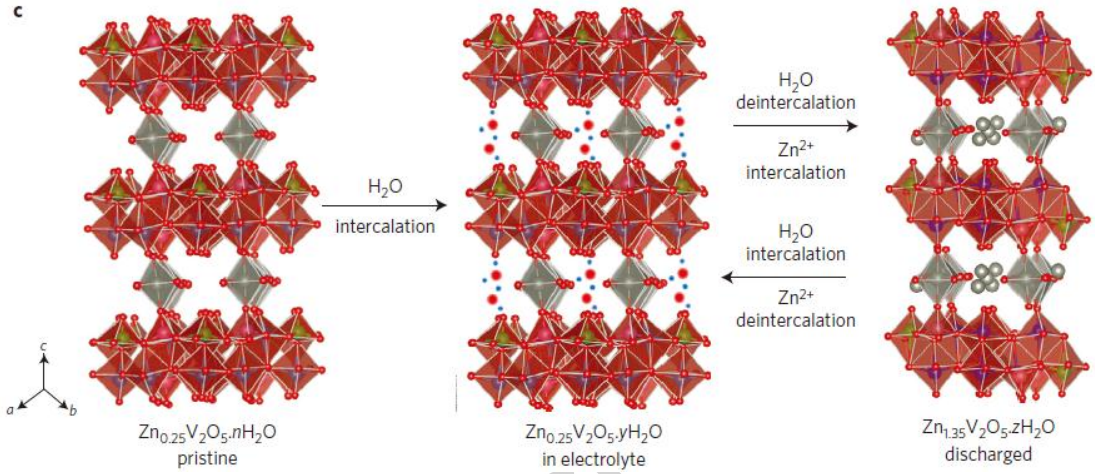

Figure 12 Scheme showing reversible water intercalation into $Zn_{0.25}V_2O_5 \cdot nH_2O$ immersed in electrolyte/H_2O, and the water deintercalation accompanying Zn^{2+} intercalation upon electrochemical discharge. The red and blue spheres represent O and H, respectively; the H_2O molecules interact with the oxygen layers through hydrogen bonding. Here y > z > n; as a fraction of intercalated H_2O remains in the discharged material. Reproduced with permission.[49] Copyright 2016, Springer Nature.

Accepted m

Another layer compound as cathode material for Zn-ion batteries is VS_2 nanosheets studied by Mai *et al.* [50]. Based on the *ex situ* XRD and *in situ* Raman results, there were two regimes in the Zn^{2+} intercalation process; 0.09 Zn^{2+} per VS_2 was inserted in the first regime while 0.14 Zn^{2+} per VS_2 was inserted in the second regime. Moreover, the capacitance provided a major contribution to the total capacity based on the cyclic voltammetry (CV) results at various scanning rates, meaning Zn^{2+}

ACCEPTED MANUSCRIPT

intercalation/deintercalation mainly happened in the near surface region.

5. Al^{3+} based intercalation-type electrode materials

The first Al-ion based primary battery (called a Buff cell) was introduced in 1857 by Tommasi *et al.*, though the concept of aluminum as a cathode coupled with zinc as an anode was first put forward by Hulot *et al.* in 1850 [126, 127]. Later on, nonaqueous rechargeable Al batteries using electrolytes including molten salt at high temperature and ionic liquid at room temperature were developed [128]. Investigation of Al-ion type rechargeable aqueous batteries based on intercalation only started recently, exclusively focusing on TiO_2, V_2O_5, MoO_3 and Prussian blue analogs [56, 129-132].

Anatase TiO_2 is widely used in aqueous LIBs and NIBs benefitting from its chemical stability and environmental friendliness. Compared with the radius of 76 pm for Li^+ cation and 102 pm for Na^+ cation, the much smaller size of 53.5 pm for Al^{3+} cation endows Al^{3+} with the potential for more favorable intercalation into the TiO_2 structure. Anatase TiO_2 nanotubes prepared by anodizing the metallic titanium foil were investigated with CV by Gao *et al.* in 2012 and are shown in **Figure 13a** [55]. Compared with Mg^{2+} and Li^+, Al^{3+} showed a much stronger intercalation behavior due to the size effect, the mechanism of which was further revealed by CVs under different scanning rates. As shown in **Figure 13b,** Al^{3+} intercalation was a process controlled by solid phase diffusion, rather than surface-confined charge transfer. Compared with Li^+, there was less structure distortion during the Al^{3+} intercalation, since the required number of Al^{3+} is only one-third of Li^+ to make the total charge balanced at the end of discharge.

Accepted manuscript

ACCEPTED MANUSCRIPT

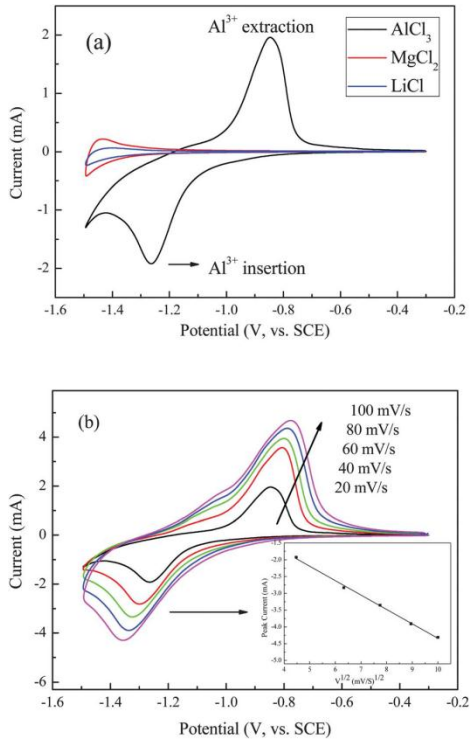

Figure 13 Typical CVs of the as-prepared anatase TiO_2 nanotube arrays in 1 M $AlCl_3$, $MgCl_2$ and LiCl aqueous solutions at 20 mV/s (a) and CVs in 1Maqueous $AlCl_3$ solution at different scan rates (b). Inset in (b) is the relationship between the cathodic peak currents and scan rates. Reproduced with permission.[55] Copyright 2012, Royal Society of Chemistry.

In the above work, the long cycling performance is not satisfied due to the irreversible Ti^{2+} formation in the discharge process, rather than the ideal reversible Ti^{3+} formation. To solve this problem, Tong *et al.* in 2014 reported black mesoporous anatase TiO_2 containing electro-conducting Ti^{3+} as cathode materials [133]. The existence of N and H in the Ti^{3+}-containing structure suppressed the formation of Ti^{2+}, resulting in a more stable cycling life. Moreover, the overall capacity in the discharge process of Ti^{3+}-containing anatase TiO_2 came from interstitial octahedral site intercalation and interfacial site storage in **Figure 14**. This result explains why the overall capacity for Ti^{3+} containing anatase TiO_2 was about 278.1 mAh/g, much higher than 77.2 mAh/g for commercial TiO_2, which exhibits only interstitial intercalation.

Accepted manuscript

ACCEPTED MANUSCRIPT

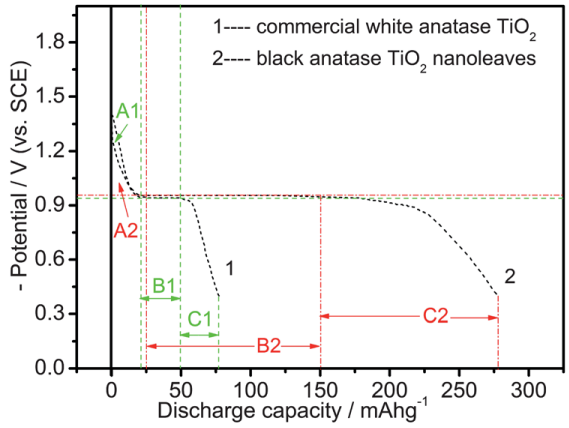

Figure 14. The first discharge profiles of black anatase TiO_2 nano leaves and commercial white anatase TiO_2 electrodes at a current rate of 0.05 A/g. Reproduced with permission.[133] Copyright 2014, Royal Society of Chemistry.

With doping electro-conducting Ti^{3+} established as a novel structural design, the associated mechanistic investigation has also progressed rapidly. Recently, Liu *et al.* hypothesized Cl^- could assist insertion and extraction of Al^{3+} [134]. Later on, the same group found co-insertion of H^+ and Al^{3+} into TiO_2 happens at the same time. Around 88% of H^+ went through the surface hydroxylation process, while 12% intercalated into the lattice, which may be only in the range of tens of nanometers beneath the surface. A more detailed mechanism requires further investigation, as suggested by the authors [135].

With less crystal structural strain during the cycling compared with TiO_2, Prussian blue analogues have received intensive attention as Al^{3+} aqueous battery electrode material for stable long-term cycling performance. Copper hexacyanoferrate as an electrode for Al^{3+} cation intercalation was first demonstrated by Chiang *et al.* [136]. The calculated Al/Cu ratio from energy dispersive x-ray spectroscopy (EDX) at different states of charge increased with Al^{3+} intercalation, while it decreased with Al^{3+} deintercalation as shown in **Figure 15e**. The Al element was distributed throughout the structure together with Fe and Cu elements in **Figure 15c**, indicating the corresponding galvanostatic charge/discharge process was not only a surface

Accepted manuscript

pseudocapacitive behavior. D-spacing changes further confirmed the intercalation behavior via a single-phase solid solution pathway between Al^{3+} and copper hexacyanoferrate.

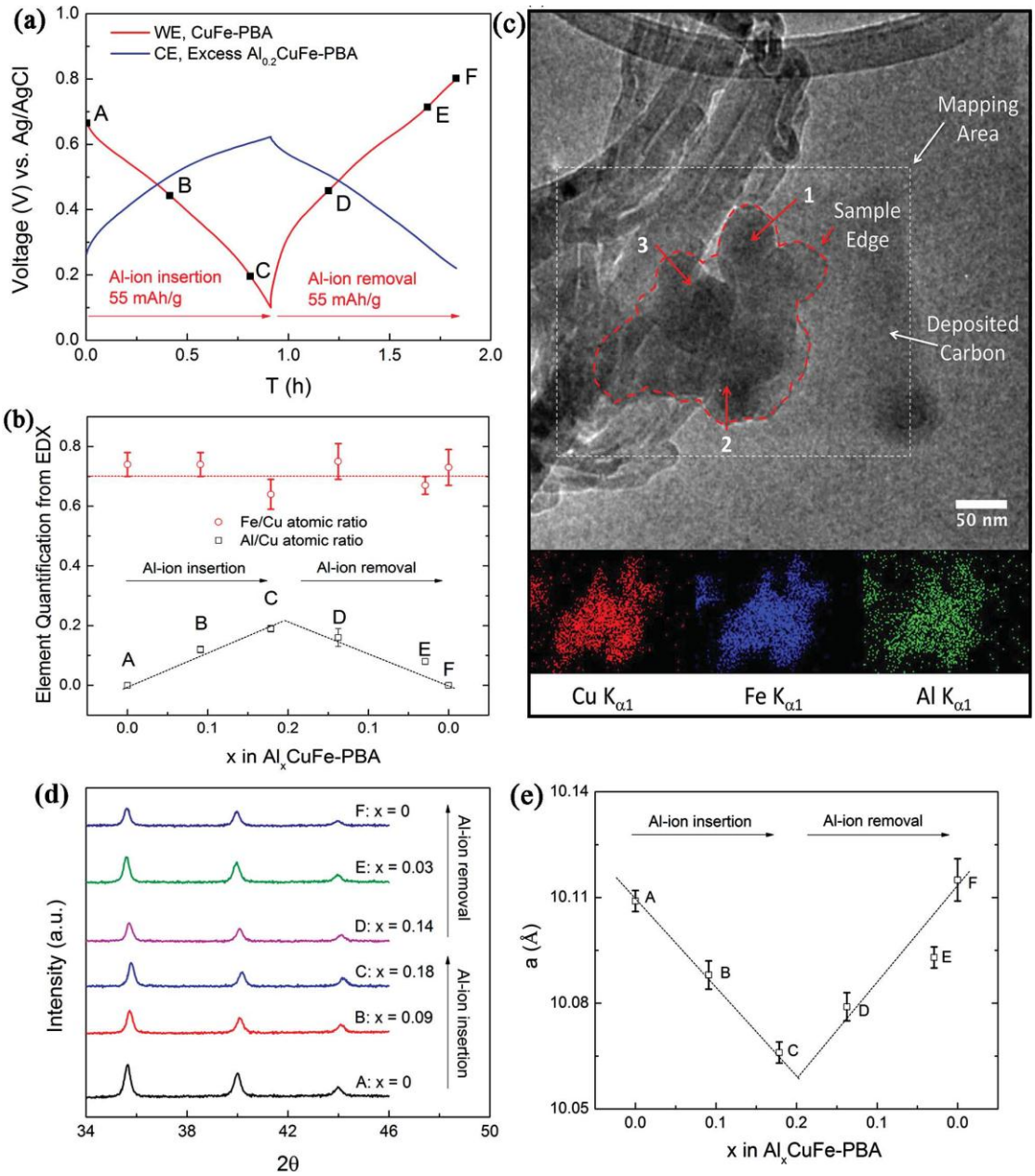

Figure 15. (a) The first discharge and charge voltage profiles (vs. Ag/AgCl) of the Al_xCuFe–PBA(CE)/CuFe–PBA(WE) three-electrode cell with respect to time. Samples A–F with various Al content at different DODs and SOCs were characterized. (b) The Al/Cu and Fe/Cu atomic ratios of samples A–F obtained from TEM EDX elemental analyses of three different points in each sample. (c) TEM EDX elemental

ACCEPTED MANUSCRIPT

mapping of sample C. (d) *Ex situ* XRD patterns of samples A–F. (e) Lattice parameter variation with Al concentration in samples A–F. Reproduced with permission.[136] Copyright 2015, Wiley-VCH.

Another investigation regarding Al^{3+} intercalated Prussian blue analogues was reported by Gao *et al.* [57]. Zeolitic water inside the structure decreased the attraction between Al^{3+} and the charged host network, therefore causing Al^{3+} diffusion kinetics to increase. Moreover, the size of the hydrated Al^{3+} was about 0.48 nm, much larger than the size of the channels in Prussian blue analogues, so dehydration occurred before Al^{3+} was inserted into the channels,. Also, the process of hydration and dehydration of Al^{3+} was affected by other anions in the solution, such as Cl^- and NO_3^-.

Unlike the stiff channel-type electrode materials such as TiO_2, layer compounds have attracted increasing attention due to their adaptable structure changes during intercalation and deintercalation. Ultrathin graphite nanosheet was demonstrated as a suitable anode material for Al^{3+} intercalation in a Zn/graphite full cell by Wu *et al.* [58]. High-resolution transmission electron microscopy (HRTEM) images confirmed the Al^{3+} intercalation. Compared with the lattice fringes of pristine graphite nanosheet in **Figure 16** a-c, the layers near the surface after discharge became wrinkled, corresponding to a d-spacing increase, while the interior domain was kept intact. These changes proved Al^{3+} intercalation into graphite nanosheets occurred, but only in the near-surface zones. Furthermore, results from CV tests under various scanning rates revealed Al^{3+} intercalation into graphite was a mix of a diffusion-controlled intercalation reaction and a surface-controlled diffusion reaction, albeit closer to the latter.

Accepted manuscript

ACCEPTED MANUSCRIPT

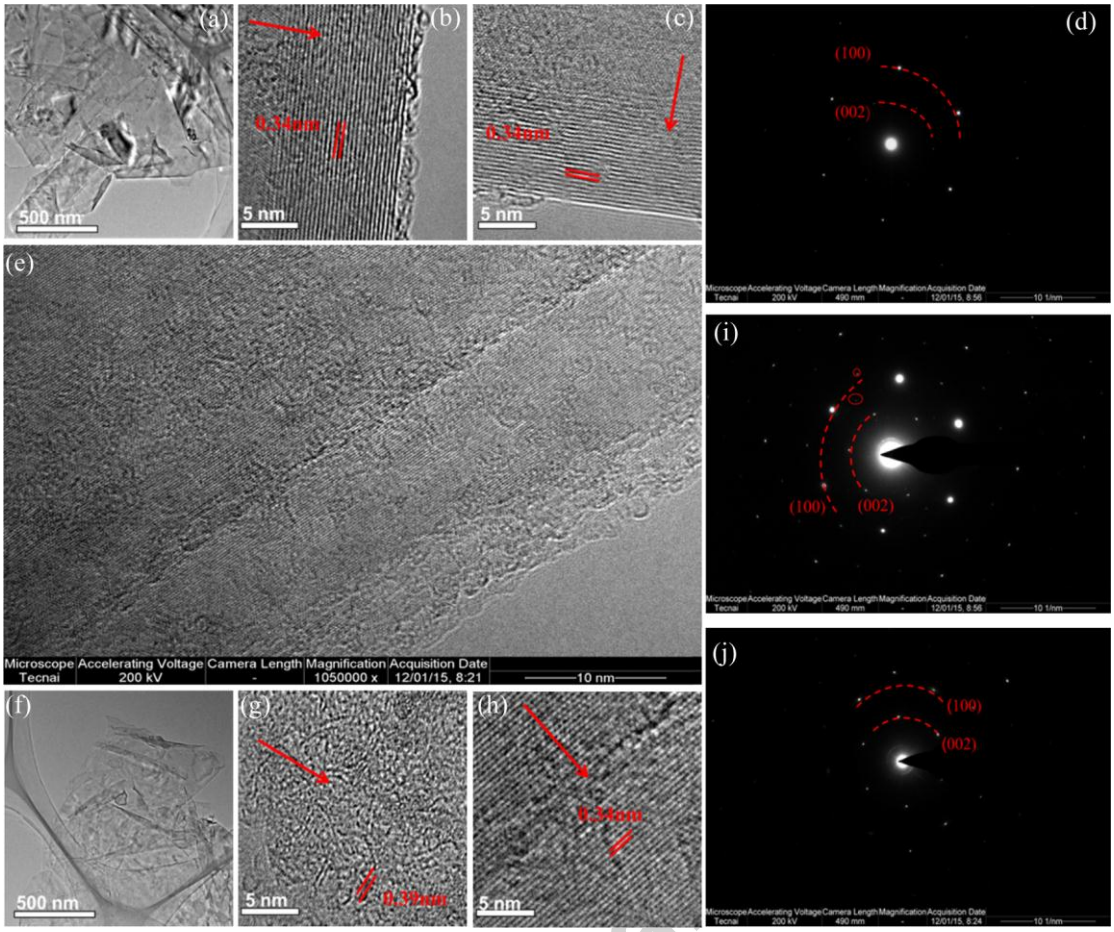

Figure 16. (a−c) HRTEM micrograph of original graphite nanosheet electrode and (d) corresponding SAED image and (e−h) HRTEM micrograph of the graphite nanosheet electrode after discharging −0.4 V (versus SCE) and (i and j) corresponding SAED images. The arrows indicate the direction along interlayer spacing. Reproduced with permission.[58] Copyright 2016, American Chemical Society.

Compared with graphite nanosheets, polypyrrole coated MoO_3 showed a similar surface controlled diffusion and bulk state diffusion in the electrochemical reaction between Al^{3+} and MoO_3 [56]. From the lack of new distinct peaks appearing after a full discharge in the *ex situ* XRD result, the authors concluded that bulk state diffusion of Al^{3+} was closer to a solid solution reaction, consistent with the slope of the galvanostatic curve in the charge/discharge process.

The mechanism of Al^{3+} intercalation into V_2O_5 seems much more complicated than that for graphite and MoO_3. Co-insertion of Al^{3+} cations, protons, and H_2O

molecules into V_2O_5 competed with chemical exchanges among them, leading to an overestimation of the content of inserted Al^{3+} and discrepancy of discharge/charge capacity at lower current density. The authors also found the capacity fading should mainly be attributed to the dissolution of V_2O_5 into the electrolyte [54].

6. Other metal cations based intercalation-type electrode materials

Many other cations, such as Rb^+, Ca^{2+}, Sr^{2+}, Ba^{2+}, Cu^{2+}, Ni^{2+}, Pb^{2+}, Y^{3+}, and La^{3+}, have also been investigated as shuttling ions for rechargeable aqueous batteries [43, 59, 60, 63, 137-140]. Especially, Prussian blue analogue and MnO_2 are demonstrated to be a versatile host for the intercalation of the above cations. Here, it should be noted insertion of Cu^{2+} into MnO_2 is more complex, especially coupled with Bi_2O_3 as an additive [137]. As shown in **Figure 17,** the host MnO_2 is reduced to $Mn(OH)_2$ while the intercalant Cu^{2+} is reduced to metallic copper in the discharge process, which is entirely different from the typical intercalation reactions between host and intercalants [59].

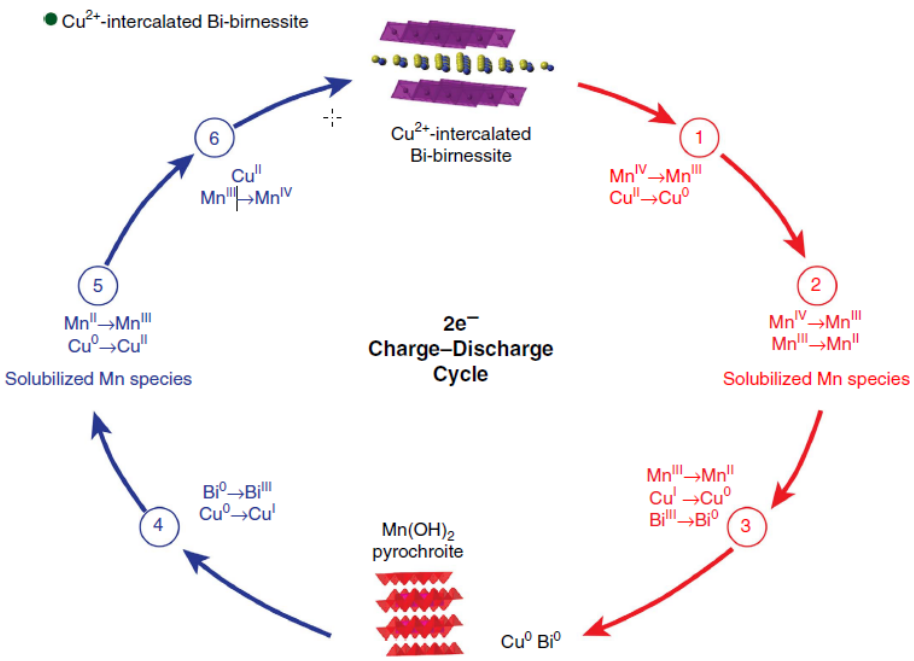

Figure 17 Schematic for electrochemical reactions for the regeneration cycle of Cu^{2+}-intercalated Bi-birnessite. Reproduced with permission.[59] Copyright 2017,

ACCEPTED MANUSCRIPT

Springer Nature.

7. Nonmetal cations intercalation-type electrode material

Many electrochemical reactions in aqueous batteries require H_3O^+ as a reactant. For instance, MnO_2 and $Ni(OH)_2$ act as cathodes in the alkaline electrolyte, quinone as an anode in the acid and alkaline electrolyte, and PbO_2 as a cathode in the acid electrolyte [141-147]. It should be noted that the studies mentioned above are all based on conversion reactions, during which the structure reassembly and volume breath result in severe capacity fading in these aqueous batteries. Moreover, cation co-intercalation with H_3O^+ has also been identified [45, 46, 48, 99, 100, 148]. Wang *et al.* revealed that H_3O^+ could co-insert into MnO_2 with Zn^{2+} in mildly acidic $ZnSO_4/MnSO_4$ electrolyte [149]. Based on the *ex situ* galvanostatic intermittent titration technique, electrochemical impedance spectroscopy and XRD results, the authors concluded that H_3O^+ intercalation happened first followed by Zn^{2+} intercalation in the discharge process.

Nevertheless, aqueous batteries entirely based on H_3O^+ intercalation chemistry have never been reported before. Recently, Ji *et al.* demonstrated that hydronium ions could be intercalated into PTCDA reversibly for the first time [61]. The structure lattices were expanded or contracted upon hydronium's intercalation or deintercalation based on the ex-situ XRD and density functional theory calculations. A reversible capacity around 85 mAh/g was obtained at a current density of 1 A/g after initial conditioning cycles.

In comparison with H_3O^+, NH_4^+ has a smaller hydrated ionic size, thus facilitating better diffusion kinetics. Cui *et al.* first studied NH_4^+ as a carrier for aqueous battery in copper hexacyanoferrate and nickel hexacyanoferrate electrodes, though NH_4^+ showed inferior performance compared with Li^+, $Na^{+,}$ and K^+ [62]. Later on, the intercalation behavior of NH_4^+ into Mxene was reported by Gogotsi *et al.* [150]. Recently, Ji *et al.* reported a NH_4-ion rocking-chair battery, utilizing

Accepted manuscript

ACCEPTED MANUSCRIPT

$(NH_4)_{1.47}Ni[Fe(CN)_6]_{0.88}$ as the cathode and PTCDI as the anode [63]. The full cell delivered a high energy density of 43 Wh/kg with 67% capacity retention after 1000 cycles. The cathode material and anode material took advantage of the fixed channel from Prussian blue analogue and flexible interlayer spacing from weak van der Waals' forces, respectively.

8. Challenges and Perspectives

So far, we have summarized the aqueous intercalation-type electrode materials beyond those hosting only Li^+ and Na^+, including the intercalants NH_4^+, H^+, K^+, Mg^{2+}, Zn^{2+}, Rb^+, Ca^{2+}, Sr^{2+}, Ba^{2+}, Cu^{2+}, Ni^{2+}, Pb^{2+}, Y^{3+}, La^{3+}, and Al^{3+}. Among these cations, only K^+, Mg^{2+}, Zn^{2+}, and Al^{3+} have been widely investigated. Moreover, the number of known host materials is relatively small, and only MnO_2, MoO_3, V_2O_5, VS_2 TiO_2, $Na_3V_2(PO_4)_3$, $Zn_{0.25}V_2O_5{\cdot}nH_2O$, $ZnMn_2O_4$, PTCDA, PTCDI, Prussian blue and its analogues have been reported so far. Compared with the available intercalation-type electrode materials for aqueous LIBs and NIBs, the electrode materials for these cations are extremely limited. Therefore, continuous research to explore more host materials is in need, and special attention should be focused on compounds, within stable aqueous electrolytes voltage window, containing appropriate interstitial sites or suitable interlayer spacing.

Besides expanding the scope of host materials, the intercalation mechanism should also be further plumbed. As we have summarized, the mechanism of Zn^{2+} intercalation into α-MnO_2 is under debate by different groups, and even the discharged products cannot be confirmed confidently. Moreover, the electrochemical reactions in the aqueous electrolyte are much more complicated than those in the organic electrolyte. While researchers are aware that water solvation and desolvation play significant roles during the intercalation and deintercalation process, a detailed and reliable description is still absent. On one hand, a facile intercalation process may be possible due to the screening effect of solvated cations;

Accepted manuscript

ACCEPTED MANUSCRIPT

on the other hand, the enlarged size of solvated cations may impede the diffusion inside the lattice. Thus, an overall evaluation of the solvation effects is required. Additionally, proton co-intercalation as charge compensation has not been well investigated, though proton co-intercalation, into the deintercalated electrode materials in acidic solution, is believed to deteriorate the long cycling performance of aqueous LIBs. It should be noted that proton co-intercalation may behave differently under similar pH or voltage windows in these aqueous batteries. Therefore, a thorough and systematic investigation based on advanced characterization techniques is in demand to elucidate the above query.

Compared with the relatively inert nature of organic electrolytes, aqueous electrolytes are so reactive that more side reactions may happen. First, the narrow aqueous electrolyte window is only 1.23V, though the kinetic factors may push the limit to 2 V in some cases. However, some electrode materials themselves can act as the catalyst for HER or OER, such as V_2O_5 for OER and VS_2 for HER, shrinking the effective voltage window and leading to a dramatically lowered energy density [151, 152]. Second, the solid-electrolyte interface formed under decomposition of organic electrolytes can further protect electrode materials, while the formed H_2 or O_2 from H_2O has no beneficial effect at all. On the contrary, O_2 may oxidize the discharged anode material. Finally, co-intercalation of protons or H_2O makes the situation more complicated. Apart from the elusive mechanism we discussed above, the changing pH with co-intercalated or co-deintercalated protons may facilitate the dissolution of certain electrode materials, especially at the nanoscale. However, nanomaterials are still the ideal choice with the higher power density with faster diffusion kinetics and better cycling performance due to less structural distortions, compared with bulk materials.

Accepted manuscript

ACCEPTED MANUSCRIPT

Table 2 List of cation radii for six-coordination [153, 154]

Cation	Ionic radius (pm)	Cation	Ionic radius (pm)
Li^+	76	Zn^{2+}	74
H_3O^+	100	Ca^{2+}	100
Na^+	102	Sr^{2+}	118
K^+	138	Pb^{2+}	119
NH_4^+	148	Ba^{2+}	135
Ni^{2+}	70	Al^{3+}	53
Mg^{2+}	72	Y^{3+}	90
Cu^{2+}	73	La^{3+}	103

GES plays a central role in mitigating the imbalance between intermittent electricity produced by renewable energy sources and varied practical electricity need. Thus, low cost, high safety, and stable cycling performance are the most fundamental requirements. The aqueous battery system itself can fulfill the low cost and high safety demand, but superior cycling stability remains the major hurdle for commercial success. As is pointed out in the above discussion, there are two effective strategies should be considered, including choosing suitable electrode materials and optimizing electrolyte composition. Among various electrode materials for the aqueous battery system, intercalatable materials are good candidates due to their reversible structure changes during cycling, including compounds with fixed interstitial sites or flexible interlayer spaces. In particular, electrode materials for multivalent cation intercalation should receive more attention. It is because the required number of multivalent cations is significantly reduced compared with monovalent cations for a charged host structure, thus resulting in less structural strain during cycling. Moreover, the ionic size of multivalent cations shown in **Table 2** is usually smaller than that of monovalent cations, facilitating a faster diffusion process [155]. Besides choosing suitable electrode materials, suppression of side reactions such as OER, HER and electrode dissolution with changing pH should also receive equal focus. As we know, electrolyte is another important factor in the batteries beyond the electrode materials, which is not covered in this review paper and should be

Accepted manuscript

ACCEPTED MANUSCRIPT

systematically discussed somewhere else. Taken all together, continued efforts should be made to develop suitable electrode materials and optimize electrolyte composition, making GES with low cost, high safety and stable cycling into a reality.

Acknowledgment

The authors express their appreciation to the University of Waterloo, Natural Sciences and Engineering Research Council of Canada (NSERC) and the Waterloo Institute for Nanotechnology for their financial support. The authorship also gratefully acknowledges financial support from the National Natural Science Foundation of China (51272182, 51772219, 21471116, and 51641210), the Zhejiang Provincial Natural Science Foundation of China (LZ17E020002 and LZ15E020002), and the Wenzhou Scientific and Technological in Public Project (G20170018).

Reference

[1] C. Patel, E. Burkhardt, C. Lambert, Science, 184 (1974) 1176.
[2] J.C. Zachos, G.R. Dickens, R.E. Zeebe, Nature, 451 (2008) 279.
[3] S. Shafiee, E. Topal, Energy policy, 37 (2009) 181.
[4] T.B. Johansson, L. Burnham, Renewable energy: sources for fuels and electricity, Island press1993.
[5] F. Katiraei, R. Iravani, N. Hatziargyriou, A. Dimeas, IEEE power and energy magazine, 6 (2008).
[6] C. Bueno, J.A. Carta, Renewable and Sustainable Energy Reviews, 10 (2006) 312.
[7] S. Zunft, C. Jakiel, M. Koller, C. Bullough, Sixth International Workshop on Large-Scale Integration of Wind Power and Transmission Networks for Offshore Windfarms, 26-28 October 2006, Delft, the Netherlands2006, 346.
[8] H. Akagi, H. Sato, IEEE Transactions on Power Electronics, 17 (2002) 109.
[9] W. Li, A. Yu, D.C. Higgins, B.G. Llanos, Z. Chen, J Am Chem Soc, 132 (2010) 17056.
[10] Z. Chen, D. Higgins, A. Yu, L. Zhang, J. Zhang, Energ Environ Sci, 4 (2011) 3167.
[11] J.A. Turner, Science, 285 (1999) 687.
[12] N.S. Choi, Z. Chen, S.A. Freunberger, X. Ji, Y.K. Sun, K. Amine, G. Yushin, L.F. Nazar, J. Cho, P.G. Bruce, Angewandte Chemie International Edition, 51 (2012) 9994.
[13] Z. Xing, B. Wang, W. Gao, C. Pan, J.K. Halsted, E.S. Chong, J. Lu, X. Wang, W. Luo, C.-H. Chang, Nano Energy, 11 (2015) 600.
[14] J. Rogers, H. Boenig, R. Schermer, J. Hauer, IEEE Transactions on Magnetics, 21 (1985) 752.
[15] B. Dunn, H. Kamath, J.-M. Tarascon, Science, 334 (2011) 928.
[16] Z. Yang, J. Zhang, M.C. Kintner-Meyer, X. Lu, D. Choi, J.P. Lemmon, J. Liu, Chem Rev, 111 (2011) 3577.
[17] Z. Xing, Z. Jian, W. Luo, Y. Qi, C. Bommier, E.S. Chong, Z. Li, L. Hu, X. Ji, Energy Storage Materials, 2 (2016) 63.

Accepted manuscript

ACCEPTED MANUSCRIPT

[18] Z. Xing, Y. Qi, Z. Jian, X. Ji, ACS applied materials & interfaces, 9 (2016) 4343.
[19] Z. Xing, X. Luo, Y. Qi, W.F. Stickle, K. Amine, J. Lu, X. Ji, ChemNanoMat, 2 (2016) 692.
[20] G. Tan, R. Xu, Z. Xing, Y. Yuan, J. Lu, J. Wen, C. Liu, L. Ma, C. Zhan, Q. Liu, Nature Energy, 2 (2017) 17090.
[21] Z. Chang, Y. Yang, M. Li, X. Wang, Y. Wu, Journal of Materials Chemistry A, 2 (2014) 10739.
[22] F. Beck, P. Rüetschi, Electrochim Acta, 45 (2000) 2467.
[23] J.O.G. Posada, A.J. Rennie, S.P. Villar, V.L. Martins, J. Marinaccio, A. Barnes, C.F. Glover, D.A. Worsley, P.J. Hall, Renewable and Sustainable Energy Reviews, 68 (2017) 1174.
[24] J.F. Manwell, J.G. McGowan, Solar Energy, 50 (1993) 399.
[25] C.-C. Hua, M.-Y. Lin, Industrial Electronics, 2000. ISIE 2000. Proceedings of the 2000 IEEE International Symposium on, IEEE2000, 135.
[26] S. Ovshinsky, M. Fetcenko, J. Ross, Science(Washington), 260 (1993) 176.
[27] T. Sakai, H. Ishikawa, K. Oguro, C. Iwakura, H. Yoneyama, J Electrochem Soc, 134 (1987) 558.
[28] R.K. Guduru, J.C. Icaza, Nanomaterials, 6 (2016) 41.
[29] H. Kim, J. Hong, K.-Y. Park, H. Kim, S.-W. Kim, K. Kang, Chem Rev, 114 (2014) 11788.
[30] Y. Wang, J. Yi, Y. Xia, Adv Energy Mater, 2 (2012) 830.
[31] L. Chen, L. Zhang, X. Zhou, Z. Liu, Chemsuschem, 7 (2014) 2295.
[32] S. Ovshinsky, M. Fetcenko, J. Ross, Science, 260 (1993) 176.
[33] O. Caumont, P. Le Moigne, C. Rombaut, X. Muneret, P. Lenain, IEEE Transactions on Energy Conversion, 15 (2000) 354.
[34] W. Li, J.R. Dahn, D.S. Wainwright, Science-AAAS-Weekly Paper Edition-including Guide to Scientific Information, 264 (1994) 1115.
[35] A. Dushina, J. Stojadinović, F. La Mantia, Electrochim Acta, 167 (2015) 262.
[36] C.D. Wessells, R.A. Huggins, Y. Cui, Nat Commun, 2 (2011) 550.
[37] C.D. Wessells, S.V. Peddada, R.A. Huggins, Y. Cui, Nano Lett, 11 (2011) 5421.
[38] C.D. Wessells, M.T. McDowell, S.V. Peddada, M. Pasta, R.A. Huggins, Y. Cui, Acs Nano, 6 (2012) 1688.
[39] L. Chen, H. Shao, X. Zhou, G. Liu, J. Jiang, Z. Liu, Nat Commun, 7 (2016).
[40] C. Yuan, Y. Zhang, Y. Pan, X. Liu, G. Wang, D. Cao, Electrochim Acta, 116 (2014) 404.
[41] K.W. Nam, S. Kim, S. Lee, M. Salama, I. Shterenberg, Y. Gofer, J.-S. Kim, E. Yang, C.S. Park, J.-S. Kim, Nano Lett, 15 (2015) 4071.
[42] H. Zhang, K. Ye, S. Shao, X. Wang, K. Cheng, X. Xiao, G. Wang, D. Cao, Electrochim Acta, 229 (2017) 371.
[43] I.A. Rodríguez-Pérez, Y. Yuan, C. Bommier, X. Wang, L. Ma, D.P. Leonard, M.M. Lerner, R.G. Carter, T. Wu, P.A. Greaney, J Am Chem Soc, 139 (2017) 13031.
[44] B. Lee, C.S. Yoon, H.R. Lee, K.Y. Chung, B.W. Cho, S.H. Oh, Sci Rep-Uk, 4 (2014).
[45] J. Lee, J.B. Ju, W.I. Cho, B.W. Cho, S.H. Oh, Electrochim Acta, 112 (2013) 138.
[46] M.H. Alfaruqi, V. Mathew, J. Gim, S. Kim, J. Song, J.P. Baboo, S.H. Choi, J. Kim, Chem Mater, 27 (2015) 3609.
[47] C. Wei, C. Xu, B. Li, H. Du, F. Kang, J Phys Chem Solids, 73 (2012) 1487.
[48] N. Zhang, F. Cheng, Y. Liu, Q. Zhao, K. Lei, C. Chen, X. Liu, J. Chen, J Am Chem Soc, 138 (2016) 12894.
[49] D. Kundu, B.D. Adams, V. Duffort, S.H. Vajargah, L.F. Nazar, Nature Energy, 1 (2016) 16119.
[50] P. He, M. Yan, G. Zhang, R. Sun, L. Chen, Q. An, L. Mai, Adv Energy Mater, 7 (2017).

Accepted manuscript

ACCEPTED MANUSCRIPT

[51] G. Li, Z. Yang, Y. Jiang, C. Jin, W. Huang, X. Ding, Y. Huang, Nano Energy, 25 (2016) 211.
[52] R. Trócoli, F. La Mantia, Chemsuschem, 8 (2015) 481.
[53] L. Zhang, L. Chen, X. Zhou, Z. Liu, Sci Rep-Uk, 5 (2015) 18263.
[54] J. González, F. Nacimiento, M. Cabello, R. Alcántara, P. Lavela, J. Tirado, RSC Advances, 6 (2016) 62157.
[55] S. Liu, J. Hu, N. Yan, G. Pan, G. Li, X. Gao, Energ Environ Sci, 5 (2012) 9743.
[56] F. Wang, Z. Liu, X. Wang, X. Yuan, X. Wu, Y. Zhu, L. Fu, Y. Wu, Journal of Materials Chemistry A, 4 (2016) 5115.
[57] S. Liu, G. Pan, G. Li, X. Gao, Journal of Materials Chemistry A, 3 (2015) 959.
[58] F. Wang, F. Yu, X. Wang, Z. Chang, L. Fu, Y. Zhu, Z. Wen, Y. Wu, W. Huang, ACS applied materials & interfaces, 8 (2016) 9022.
[59] G.G. Yadav, J.W. Gallaway, D.E. Turney, M. Nyce, J. Huang, X. Wei, S. Banerjee, Nat Commun, 8 (2017).
[60] R.Y. Wang, B. Shyam, K.H. Stone, J.N. Weker, M. Pasta, H.W. Lee, M.F. Toney, Y. Cui, Adv Energy Mater, 5 (2015).
[61] X. Wang, C. Bommier, Z. Jian, Z. Li, R.S. Chandrabose, I.A. Rodríguez - Pérez, P.A. Greaney, X. Ji, Angewandte Chemie, 129 (2017) 2955.
[62] C.D. Wessells, S.V. Peddada, M.T. McDowell, R.A. Huggins, Y. Cui, J Electrochem Soc, 159 (2011) A98.
[63] X. Wu, Y. Qi, J.J. Hong, Z. Li, A.S. Hernandez, X. Ji, Angewandte Chemie, 129 (2017) 13206.
[64] J.W. McCargar, V.D. Neff, The Journal of Physical Chemistry, 92 (1988) 3598.
[65] V.D. Neff, J Electrochem Soc, 125 (1978) 886.
[66] E. Grabner, S. Kalwellis-Mohn, Journal of applied electrochemistry, 17 (1987) 653.
[67] V.D. Neff, J. Electrochem. Soc.;(United States), 132 (1985).
[68] D. Su, A. McDonagh, S.Z. Qiao, G. Wang, Adv Mater, 29 (2017).
[69] M. Pasta, C.D. Wessells, R.A. Huggins, Y. Cui, Nat Commun, 3 (2012) 1149.
[70] S. Kalwellis-Mohn, E. Grabner, Electrochim Acta, 34 (1989) 1265.
[71] S. Sinha, B.D. Humphrey, A.B. Bocarsly, Inorg Chem, 23 (1984) 203.
[72] P. Jiang, H. Shao, L. Chen, J. Feng, Z. Liu, Journal of Materials Chemistry A, 5 (2017) 16740.
[73] C. Liu, X. Wang, W. Deng, C. Li, J. Chen, M. Xue, R. Li, F. Pan, Angewandte Chemie, (2018).
[74] R. Bors, J. Yun, P. Marzak, J. Fichtner, D. Scieszka, A.S. Bandarenka, ACS Omega, 3 (2018) 5111.
[75] N.D. Schuppert, S. Mukherjee, A.M. Bates, E.-J. Son, M.J. Choi, S. Park, J Power Sources, 316 (2016) 160.
[76] T.D. Gregory, R.J. Hoffman, R.C. Winterton, J Electrochem Soc, 137 (1990) 775.
[77] P. Novak, J. Desilvestro, J Electrochem Soc, 140 (1993) 140.
[78] L. Chen, J.L. Bao, X. Dong, D.G. Truhlar, Y. Wang, C. Wang, Y. Xia, ACS Energy Letters, 2 (2017) 1115.
[79] R.Y. Wang, C.D. Wessells, R.A. Huggins, Y. Cui, Nano Lett, 13 (2013) 5748.
[80] Y. Mizuno, M. Okubo, E. Hosono, T. Kudo, H. Zhou, K. Oh-ishi, The Journal of Physical Chemistry C, 117 (2013) 10877.
[81] B. Winther-Jensen, M. Gaadingwe, D. Macfarlane, M. Forsyth, Electrochim Acta, 53 (2008) 5881.
[82] I. Stojković, N. Cvjetićanin, S. Marković, M. Mitrić, S. Mentus, Acta Physica Polonica A, 117 (2010) 837.

Accepted manuscript

ACCEPTED MANUSCRIPT

[83] M. Vujković, I. Pašti, I.S. Simatović, B. Šljukić, M. Milenković, S. Mentus, Electrochim Acta, 176 (2015) 130.

[84] C. Kim, P.J. Phillips, B. Key, T. Yi, D. Nordlund, Y.S. Yu, R.D. Bayliss, S.D. Han, M. He, Z. Zhang, Adv Mater, 27 (2015) 3377.

[85] H. Zhang, K. Ye, K. Zhu, R. Cang, J. Yan, K. Cheng, G. Wang, D. Cao, Chem-Eur J, (2017).

[86] H. Zhang, K. Ye, K. Zhu, R. Cang, X. Wang, G. Wang, D. Cao, ACS Sustainable Chemistry & Engineering, 5 (2017) 6727.

[87] K. Vuorilehto, Journal of applied electrochemistry, 33 (2003) 15.

[88] H. Zhang, K. Ye, K. Zhu, R. Cang, J. Yan, K. Cheng, G. Wang, D. Cao, Electrochim Acta, 256 (2017) 357.

[89] H. Zhang, K. Ye, K. Zhu, R. Cang, J. Yan, K. Cheng, G. Wang, D. Cao, Chem-Eur J, 23 (2017) 17118.

[90] H. Zhang, K. Ye, R. Cang, K. Zhu, J. Yan, K. Cheng, G. Wang, D. Cao, Journal of Electroanalytical Chemistry, 807 (2017) 37.

[91] Z. Jia, J. Hao, L. Liu, Y. Wang, T. Qi, Ionics, (2018) 1.

[92] H. Zhang, K. Ye, X. Huang, X. Wang, K. Cheng, X. Xiao, G. Wang, D. Cao, J Power Sources, 338 (2017) 136.

[93] F. Wang, X. Fan, T. Gao, W. Sun, Z. Ma, C. Yang, F. Han, K. Xu, C. Wang, ACS central science, 3 (2017) 1121.

[94] M.H. Alfaruqi, S. Islam, J. Gim, J. Song, S. Kim, D.T. Pham, J. Jo, Z. Xiu, V. Mathew, J. Kim, Chem Phys Lett, 650 (2016) 64.

[95] M.H. Alfaruqi, J. Gim, S. Kim, J. Song, J. Jo, S. Kim, V. Mathew, J. Kim, J Power Sources, 288 (2015) 320.

[96] M.H. Alfaruqi, S. Islam, V. Mathew, J. Song, S. Kim, D.P. Tung, J. Jo, S. Kim, J.P. Baboo, Z. Xiu, Applied Surface Science, 404 (2017) 435.

[97] N. Zhang, F. Cheng, J. Liu, L. Wang, X. Long, X. Liu, F. Li, J. Chen, Nat Commun, 8 (2017).

[98] H. Pan, Y. Shao, P. Yan, Y. Cheng, K.S. Han, Z. Nie, C. Wang, J. Yang, X. Li, P. Bhattacharya, Nature Energy, 1 (2016) 16039.

[99] B. Lee, H.R. Lee, H. Kim, K.Y. Chung, B.W. Cho, S.H. Oh, Chem Commun, 51 (2015) 9265.

[100] C. Xu, B. Li, H. Du, F. Kang, Angewandte Chemie International Edition, 51 (2012) 933.

[101] D. Kundu, P. Oberholzer, C. Glaros, A. Bouzid, E. Tervoort, A. Pasquarello, M. Niederberger, Chem Mater, (2018).

[102] C. Zhu, G. Fang, J. Zhou, J. Guo, Z. Wang, C. Wang, J. Li, Y. Tang, S. Liang, Journal of Materials Chemistry A, (2018).

[103] M.H. Alfaruqi, S. Islam, D.Y. Putro, V. Mathew, S. Kim, J. Jo, S. Kim, Y.-K. Sun, K. Kim, J. Kim, Electrochim Acta, (2018).

[104] N. Qiu, H. Chen, Z. Yang, S. Sun, Y. Wang, RSC Advances, 8 (2018) 15703.

[105] T. Wei, Q. Li, G. Yang, C. Wang, Journal of Materials Chemistry A, 6 (2018) 8006.

[106] Z. Wang, Z. Ruan, Z. Liu, Y. Wang, Z. Tang, H. Li, M. Zhu, T.F. Hung, J. Liu, Z. Shi, Journal of Materials Chemistry A, (2018).

[107] J. Zhou, L. Shan, Z. Wu, X. Guo, G. Fang, S. Liang, Chem Commun, 54 (2018) 4457.

[108] Z. Peng, Q. Wei, S. Tan, P. He, W. Luo, Q. An, L. Mai, Chem Commun, 54 (2018) 4041.

[109] V. Soundharrajan, B. Sambandam, S. Kim, M.H. Alfaruqi, D.Y. Putro, J. Jo, S. Kim, V. Mathew, Y.-K. Sun, J. Kim, Nano Lett, 18 (2018) 2402.

[110] Q. Pang, C. Sun, Y. Yu, K. Zhao, Z. Zhang, P.M. Voyles, G. Chen, Y. Wei, X. Wang, Adv Energy

Accepted manuscript

ACCEPTED MANUSCRIPT

Mater, (2018) 1800144.

[111] S. Zhao, B. Han, D. Zhang, Q. Huang, L. Xiao, L. Chen, D.G. Ivey, Y. Deng, W. Wei, Journal of Materials Chemistry A, 6 (2018) 5733.

[112] C. Xia, J. Guo, P. Li, X. Zhang, H.N. Alshareef, Angewandte Chemie International Edition, 57 (2018) 3943.

[113] B. Sambandam, V. Soundharrajan, S. Kim, M.H. Alfaruqi, J. Jo, S. Kim, V. Mathew, Y.-k. Sun, J. Kim, Journal of Materials Chemistry A, 6 (2018) 3850.

[114] B. Wu, G. Zhang, M. Yan, T. Xiong, P. He, L. He, X. Xu, L. Mai, Small, 14 (2018) 1703850.

[115] P. Hu, T. Zhu, X. Wang, X. Wei, M. Yan, J. Li, W. Luo, W. Yang, W. Zhang, L. Zhou, Nano Lett, 18 (2018) 1758.

[116] P. He, G. Zhang, X. Liao, M. Yan, X. Xu, Q. An, J. Liu, L. Mai, Adv Energy Mater, (2018).

[117] C. Xia, J. Guo, Y. Lei, H. Liang, C. Zhao, H.N. Alshareef, Adv Mater, 30 (2018) 1705580.

[118] P. He, Y. Quan, X. Xu, M. Yan, W. Yang, Q. An, L. He, L. Mai, Small, 13 (2017).

[119] M. Yan, P. He, Y. Chen, S. Wang, Q. Wei, K. Zhao, X. Xu, Q. An, Y. Shuang, Y. Shao, Adv Mater, 30 (2018).

[120] J. Hao, J. Mou, J. Zhang, L. Dong, W. Liu, C. Xu, F. Kang, Electrochim Acta, 259 (2018) 170.

[121] S. Islam, M.H. Alfaruqi, V. Mathew, J. Song, S. Kim, S. Kim, J. Jo, J.P. Baboo, D.T. Pham, D.Y. Putro, Journal of Materials Chemistry A, 5 (2017) 23299.

[122] V. Renman, D.O. Ojwang, M. Valvo, C.P. Gómez, T. Gustafsson, G. Svensson, J Power Sources, 369 (2017) 146.

[123] X. Wu, Y. Xiang, Q. Peng, X. Wu, Y. Li, F. Tang, R. Song, Z. Liu, Z. He, X. Wu, Journal of Materials Chemistry A, 5 (2017) 17990.

[124] Z. Jia, B. Wang, Y. Wang, Materials Chemistry and Physics, 149 (2015) 601.

[125] L. Zhang, L. Chen, X. Zhou, Z. Liu, Adv Energy Mater, 5 (2015).

[126] G.A. Elia, K. Marquardt, K. Hoeppner, S. Fantini, R. Lin, E. Knipping, W. Peters, J.F. Drillet, S. Passerini, R. Hahn, Adv Mater, 28 (2016) 7564.

[127] L. Fu, N. Li, Y. Liu, W. Wang, Y. Zhu, Y. Wu, Chinese Journal of Chemistry, 35 (2017) 13.

[128] Y. Zhao, T. VanderNoot, Electrochim Acta, 42 (1997) 3.

[129] A. Holland, R. Mckerracher, A. Cruden, R. Wills, Journal of Applied Electrochemistry, 48 (2018) 243.

[130] M. Kazazi, Z.A. Zafar, M. Delshad, J. Cervenka, C. Chen, Solid State Ionics, 320 (2018) 64.

[131] H. Lahan, R. Boruah, A. Hazarika, S.K. Das, The Journal of Physical Chemistry C, 121 (2017) 26241.

[132] H. Lahan, S.K. Das, Ionics, (2018) 1.

[133] Y.J. He, J.F. Peng, W. Chu, Y.Z. Li, D.G. Tong, Journal of Materials Chemistry A, 2 (2014) 1721.

[134] Y. Liu, S. Sang, Q. Wu, Z. Lu, K. Liu, H. Liu, Electrochim Acta, 143 (2014) 340.

[135] S. Sang, Y. Liu, W. Zhong, K. Liu, H. Liu, Q. Wu, Electrochim Acta, 187 (2016) 92.

[136] Z. Li, K. Xiang, W. Xing, W.C. Carter, Y.M. Chiang, Adv Energy Mater, 5 (2015).

[137] G.G. Yadav, X. Wei, J. Huang, J.W. Gallaway, D.E. Turney, M. Nyce, J. Secor, S. Banerjee, Journal of Materials Chemistry A, 5 (2017) 15845.

[138] C. Xu, Y. Chen, S. Shi, J. Li, F. Kang, D. Su, Sci Rep-Uk, 5 (2015).

[139] C. Lee, S.-K. Jeong, Electrochim Acta, 265 (2018) 430.

[140] S. Gheytani, Y. Liang, F. Wu, Y. Jing, H. Dong, K.K. Rao, X. Chi, F. Fang, Y. Yao, Advanced Science, 4 (2017).

Accepted manuscript

ACCEPTED MANUSCRIPT

[141] M. Minakshi, P. Singh, M. Carter, K. Prince, Electrochemical and Solid-State Letters, 11 (2008) A145.

[142] E.D. Rus, G.D. Moon, J. Bai, D.A. Steingart, C.K. Erdonmez, J Electrochem Soc, 163 (2016) A356.

[143] A.P. Malloy, S.W. Donne, J Electrochem Soc, 155 (2008) A817.

[144] M. Sterby, R. Emanuelsson, X. Huang, A. Gogoll, M. Strømme, M. Sjödin, Electrochim Acta, 235 (2017) 356.

[145] Y. Liang, Y. Jing, S. Gheytani, K.-Y. Lee, P. Liu, A. Facchetti, Y. Yao, Nat Mater, 16 (2017) 841.

[146] A. Shukla, S. Venugopalan, B. Hariprakash, J Power Sources, 100 (2001) 125.

[147] N. Yu, L. Gao, S. Zhao, Z. Wang, Electrochim Acta, 54 (2009) 3835.

[148] S.H. Kim, S.M. Oh, J Power Sources, 72 (1998) 150.

[149] W. Sun, F. Wang, S. Hou, C. Yang, X. Fan, Z. Ma, T. Gao, F. Han, R. Hu, M. Zhu, J Am Chem Soc, 139 (2017) 9775.

[150] M.R. Lukatskaya, O. Mashtalir, C.E. Ren, Y. Dall'Agnese, P. Rozier, P.L. Taberna, M. Naguib, P. Simon, M.W. Barsoum, Y. Gogotsi, Science, 341 (2013) 1502.

[151] Y. Qu, M. Shao, Y. Shao, M. Yang, J. Xu, C.T. Kwok, X. Shi, Z. Lu, H. Pan, Journal of Materials Chemistry A, 5 (2017) 15080.

[152] F.-C. Shen, Y. Wang, Y.-J. Tang, S.-L. Li, Y.-R. Wang, L.-Z. Dong, Y.-F. Li, Y. Xu, Y.-Q. Lan, ACS Energy Letters, 2 (2017) 1327.

[153] R.D. Shannon, Acta crystallographica section A: crystal physics, diffraction, theoretical and general crystallography, 32 (1976) 751.

[154] A.F. Wells, Structural inorganic chemistry, Oxford University Press2012.

[155] M. Liu, Z. Rong, R. Malik, P. Canepa, A. Jain, G. Ceder, K.A. Persson, Energ Environ Sci, 8 (2015) 964.

Zhenyu Xing graduated with B.Sc. of chemistry from Jilin University in 2012. He earned his Ph.D. in chemistry from Oregon State University in 2016 under the supervision of Prof. Xiulei Ji. Currently, he is postdoctoral fellow with Prof. Zhongwei Chen at the University of Waterloo. His research focuses on preparation, structure, property and application of porous carbon materials.

Accepted manuscript

ACCEPTED MANUSCRIPT

Shun Wang is a distinguished Professor at the College of Chemistry and Materials Engineering, Wenzhou University. His research focuses on nanostructured functional materials, including carbon-based nanocomposites, functional Te nanocrystals, and hierarchically structured and assembled materials for electrochemical energy storage and conversion technologies.

Dr. Aiping Yu is an Associate Professor at University of Waterloo. Her research interests are materials development for supercapacitors, photocatalysts and nano composites. She has published over 65 papers in peer-reviewed journals, 3 book chapters, and one book. These publications have received more than 6300 citations. Her work has been featured by major media reports such as Nature Nanotechnology, WallStreet News, Photonics.com, and Azonano.com. She has held 7 patents and provisional patents, and 2 of her patents have been licensed to industry. She is also an editorial board member of Scientific Report, nature publishing group.

Dr. Zhongwei Chen is Canada Research Chair Professor in Advanced Materials for Clean Energy at University of Waterloo. His research interests are in the development of advanced energy materials for metal-air batteries, lithiumion batteries and fuel cells. He has published 1 book, 7 book chapters and more than 150 peer reviewed journal articles with over 10,000 citations with

epted manuscript

ACCEPTED MANUSCRIPT

H-index 50 (Google Scholar). He is also listed as inventor on 15 US/international patents, with several licensed to companies in USA and Canada. He was recipient of the 2016 E. W. R Steacie Memorial Fellowship, which followed shortly upon several other prestigious honors, including the Ontario Early Researcher Award, an NSERC Discovery Supplement Award, the Distinguished Performance and the Research Excellence Awards from the University of Waterloo.

high light

1 This is the first comprehensive review paper to summarize aqueous intercalation-type electrode materials for grid-level energy storage beyond the limits of lithium and sodium.

2. This review paper focuses on cations other than Li^+ and Na^+, including K^+ based, Mg^{2+} based, Zn^{2+} based, Al^{3+} based, nonmetal cations based and other cations based.

3. Compounds with suitable channels or flexible interlayer spaces should receive more attention in the search for novel electrode materials for aqueous intercalation-type batteries.

Accepted manuscript